

GIPR-Ab/GLP-1 peptide–antibody conjugate requires brain GIPR and GLP-1R for additive weight loss in obese mice

Received: 16 October 2024

Accepted: 28 March 2025

Published online: 29 April 2025

 Check for updates

Clarissa M. Liu^{1,2}, Elizabeth A. Killion¹, Rola Hammoud³, Shu-Chen Lu¹, Renee Komorowski¹, Tongyu Liu⁴, Matt Kanke⁵, Veena A. Thomas⁶, Kevin Cook⁶, Glenn N. Sivits Jr.¹, Aerielle B. Ben¹, Larissa I. Atangan¹, Rajaa Hussien⁷, Amy Tang⁷, Artem Shkumatov⁷, Chi-Ming Li⁵, Daniel J. Drucker³ & Murielle M. Véniant¹✉

Glucose-dependent insulintropic polypeptide receptor (GIPR) and glucagon-like peptide 1 receptor (GLP-1R) are expressed in the central nervous system (CNS) and regulate food intake. Here, we demonstrate that a peptide–antibody conjugate that blocks GIPR while simultaneously activating GLP-1R (GIPR-Ab/GLP-1) requires both CNS GIPR and CNS GLP-1R for maximal weight loss in obese, primarily male, mice. Moreover, dulaglutide produces greater weight loss in CNS GIPR knockout (KO) mice, and the weight loss achieved with dulaglutide + GIPR-Ab is attenuated in CNS GIPR KO mice. Wild-type mice treated with GIPR-Ab/GLP-1 and CNS GIPR KO mice exhibit similar changes in gene expression related to tissue remodelling, lipid metabolism and inflammation in white adipose tissue and liver. Moreover, GIPR-Ab/GLP-1 is detected in circumventricular organs in the brain and activates c-FOS in downstream neural substrates involved in appetite regulation. Hence, both CNS GIPR and GLP-1R signalling are required for the full weight loss effect of a GIPR-Ab/GLP-1 peptide–antibody conjugate.

The CNS has a key role in energy balance and body weight regulation, and further understanding of how the CNS regulates energy balance can aid in the development of effective treatments for obesity. Decades of research have demonstrated that the brain integrates hormonal, metabolic, cognitive and emotional signals to maintain energy balance, and dysregulation of these neural circuits can lead to conditions such as obesity or eating disorders^{1,2}. For example, the hindbrain is responsible for integrating information necessary for energy homeostasis from diverse systems, including vagally mediated gastrointestinal signals, alterations in glucose and other circulating metabolites and descending neuroendocrine signals from the midbrain and forebrain³. In tandem,

the arcuate nucleus of the hypothalamus, which contains both anorexigenic proopiomelanocortin-expressing neurons and orexigenic agouti-related protein/neuropeptide Y-co-expressing neurons, has a key role in the homeostatic control of food intake⁴. However, energy balance is not exclusively regulated by homeostatic mechanisms. The CNS also contains ‘reward systems’ that influence motivational processes related to eating behaviour. The ventral tegmental area provides dopaminergic input to the nucleus accumbens to encode the rewarding properties of food⁵. Moreover, the consumption of palatable food increases extracellular dopamine levels in the nucleus accumbens to regulate food-seeking behaviour^{6,7}. Given all these functions,

¹Department of Cardiometabolic Disorders, Amgen Research, Thousand Oaks, CA, USA. ²Amgen R&D Postdoctoral Fellows Program, Amgen Inc., Thousand Oaks, CA, USA. ³The Department of Medicine, Lunenfeld–Tanenbaum Research Institute, Mt. Sinai Hospital, University of Toronto, Toronto, Ontario, Canada. ⁴Center for Research Acceleration by Digital Innovation, Amgen Research, Thousand Oaks, CA, USA. ⁵Department of Research Technologies, Amgen Research, South San Francisco, CA, USA. ⁶Department of Pharmacokinetics and Drug Metabolism, Amgen Research, South San Francisco, CA, USA. ⁷Department of Translational Safety and Bioanalytical Sciences, Amgen Research, South San Francisco, CA, USA. ✉e-mail: mveniant@amgen.com

identifying the mechanisms for energy balance in the CNS is important for understanding obesity as a disease and for developing effective pharmacotherapies for obesity.

Glucagon-like peptide 1 (GLP-1) and glucose-dependent insulinotropic polypeptide (GIP) are gut-derived incretin hormones that facilitate glucose-stimulated insulin secretion. In addition, both have extra-pancreatic functions that impact appetite regulation in the CNS. GLP-1 binds to receptors (GLP-1R) in the hindbrain, hypothalamus, lateral septum and cortex, engaging circuits that inhibit food intake (extensively reviewed in previous work⁸). Similarly, GIP receptor (GIPR) and GIP binding have been detected in multiple brain regions, including the hippocampus, olfactory bulb, brainstem, lateral septum and hypothalamus^{9,10}. Within the hypothalamus, *Gipr*-expressing cells are localized in the paraventricular, dorsomedial and arcuate nuclei and colocalize with markers for neurons, glia and vascular cells. Activation of the hypothalamic GIPR suppresses food intake^{11,12}. Moreover, in recent studies, chemogenetic stimulation of brainstem GIPR was also shown to suppress food intake while activating conditioned taste avoidance responses¹³.

GLP-1R and GIPR have crucial roles in metabolic homeostasis and energy balance, making them promising targets for obesity treatment. This potential is exemplified by the therapeutic efficacy of the dual agonist tirzepatide¹⁴. Additionally, novel peptide–antibody conjugates blocking GIPR and activating the GLP-1R have recently been shown to be an effective and tolerable pharmacotherapy for obesity in mice, monkeys and humans^{15,16}. The peptide–antibody conjugate GIPR-Ab/GLP-1 is a fully human monoclonal anti-human GIPR antagonist antibody (GIPR-Ab) conjugated by amino acid linkers to two GLP-1 analogues. The mechanisms engaged by this peptide–antibody conjugate leading to weight loss and metabolic improvement remain unclear. Here, we identify CNS sites activated by GIPR-Ab/GLP-1 and reveal key roles for both CNS GLP-1Rs and GIPRs to enable the full extent of weight loss and metabolic benefit.

Results

Dosing of mGIPR-Ab or mGIPR-Ab/GLP-1 produces weight loss

To investigate the role of GIPR in energy balance in the CNS, male mice that were fed a high-fat diet (HFD) were administered intracerebroventricular (ICV) injections of varying doses of a fully human anti-human GIPR antibody that cross-reacts with mouse GIPR (mGIPR-Ab). Mice were treated every other day for a total of ten doses, with daily body weight and food intake measurements (schematic of study design Fig. 1a). The dosing rationale was determined from the pharmacokinetic profile of mGIPR-Ab following a single ICV-administered dose (Extended Data Fig. 1a,b). Mice treated with 7.5, 15 and 30 µg of mGIPR-Ab lost an average of 5.1%, 9.3% and 8.2% of their initial body weight, respectively (Fig. 1b,c), whereas control mice treated with either artificial cerebrospinal fluid or two different doses of IgG1 (a non-binding control antibody) maintained a stable body weight (Fig. 1c). Cumulative food intake was significantly reduced with mGIPR-Ab treatment (Fig. 1d). Hence, medium and high doses of CNS mGIPR-Ab reduce body weight in obese mice.

We next compared ICV versus intraperitoneal (IP) administration of mGIPR-Ab in diet-induced obese (DIO) mice. Both ICV and IP administration of mGIPR-Ab led to similar magnitudes of weight loss relative to their respective controls (Fig. 1e,f and Extended Data Fig. 1c), which was accompanied by comparable reductions in cumulative food intake (Fig. 1g). Pharmacokinetic analysis revealed that mGIPR-Ab exposure in the forebrain was significantly higher with ICV administration (ICV_{avg} , 3,469 ng g⁻¹; IP_{avg} , 923.3 ng g⁻¹; Fig. 1h). On the other hand, mGIPR-Ab exposure in the hindbrain was significantly higher with IP administration (ICV_{avg} , 186.5 ng g⁻¹; IP_{avg} , 884.0 ng g⁻¹; Fig. 1i). Overall, mGIPR-Ab exposure in the whole brain was not significantly different between ICV and IP routes of administration (ICV_{avg} , 3,655 ng g⁻¹; IP_{avg} , 1,807 ng g⁻¹; Fig. 1j). As expected, mGIPR-Ab exposure in the plasma

(ICV_{avg} , 14,383 ng g⁻¹; IP_{avg} , 374,067 ng g⁻¹), inguinal white adipose tissue (WAT) (ICV_{avg} , 158.5 ng g⁻¹; IP_{avg} , 5,496 ng g⁻¹) and epididymal WAT (ICV_{avg} , 268.3 ng g⁻¹; IP_{avg} , 15,423 ng g⁻¹) was higher with IP administration (Fig. 1k–m). To determine whether these exposure levels result in significant changes in GIPR function, a cAMP assay was used to determine the IC_{50} of mGIPR-Ab in mouse Neuro2A cells (Extended Data Fig. 1d) and then compared to in vivo exposure levels. The results indicate that low exposure levels (~100 ng g⁻¹) in the hindbrain and peripheral tissues are probably meaningful and may contribute to the effects of mGIPR-Ab on body weight. Altogether, these results demonstrate that CNS GIPR antagonism leads to body weight loss, and both central and systemic dosing of mGIPR-Ab can target the CNS to regulate body weight. Moreover, following systemic administration, mGIPR-Ab has access to the brain and results in weight loss comparable to central administration of mGIPR-Ab.

We next examined the effect of mGIPR-Ab/GLP-1 on body weight using two previously characterized molecules of mGIPR-Ab/GLP-1 (mGIPR-Ab/P1 (ref. 16) and mGIPR-Ab/P3 (ref. 15)). These molecules are similar and used interchangeably for both central and peripheral administration. They consist of identical mGIPR-Ab and differ only slightly in the conjugated GLP-1 moiety but demonstrate comparable in vitro potency at both receptors (Extended Data Fig. 2a–c).

DIO mice received 1, 5, 10 or 25 µg per µl per mouse of mGIPR-Ab/P3 or 25 µg per µl per mouse of IgG1 control injected ICV every 4 days for five treatments, with body weight and food intake monitored for 44 days. ICV IgG1-treated mice maintained stable body weight, while all doses of ICV mGIPR-Ab/P3 led to substantial weight loss (Extended Data Fig. 3a,b). The highest dose resulted in an average weight loss of 31.9% by day 18, with durable weight reduction remaining evident 28 days after the final dose. These findings were associated with a significant reduction in daily food intake (Extended Data Fig. 3c). Hence, central administration of mGIPR-Ab/P3 produces significant and prolonged weight loss in obese mice.

CNS GIPR KO mice resist development of diet-induced obesity

To generate CNS-specific GIPR KO mice, *Gipr*^{fl/fl} mice¹⁷ were crossed to synapsin-Cre mice (Jackson Laboratories) to obtain *Gipr*^{fl/fl} control mice and *Gipr*^{Syn-/-} mice (breeding schematic in Fig. 2a). Synapsin is exclusively expressed in neurons, and confirmation of *Gipr* KO revealed that *Gipr* expression was lower in the brainstem, hypothalamus and hippocampus of *Gipr*^{Syn-/-} mice than in *Gipr*^{fl/fl} control mice, while *Gipr* expression in pancreatic islets was similar between the two genotypes (Fig. 2b,c). After 12 weeks of HFD feeding, *Gipr*^{Syn-/-} mice demonstrated significantly lower body weight (Fig. 2d), food intake (Fig. 2e), fat mass (Fig. 2f) and lean mass (Fig. 2g) than *Gipr*^{fl/fl} control mice, indicating that CNS GIPR has an important role in body weight gain in the context of an obesogenic diet. For comparison with published CNS GIPR KO models¹⁸ and CNS GLP-1R KO models^{19,20}, *Gipr*^{Syn-/-} mice were further characterized in two independent cohorts (Extended Data Fig. 4). There was no significant difference in plasma total cholesterol, triglycerides, high density lipoprotein cholesterol, low density lipoprotein cholesterol, leptin, adiponectin, resistin or interleukin-6 in *Gipr*^{Syn-/-} mice compared to *Gipr*^{fl/fl} mice, although plasma tumour necrosis factor (TNF) and monocyte chemoattractant protein-1 (MCP-1) were lower in *Gipr*^{Syn-/-} mice than in *Gipr*^{fl/fl} mice (Extended Data Fig. 4a–j).

We next investigated whether mGIPR-Ab modulates food intake and body weight in HFD-fed *Gipr*^{Syn-/-} mice. The reductions in body weight (Extended Data Fig. 5a,b) and food intake (Extended Data Fig. 5c) following IP mGIPR-Ab treatment were absent in *Gipr*^{Syn-/-} mice yet preserved in *Gipr*^{fl/fl} control mice. mGIPR-Ab treatment had no impact on fat mass (Extended Data Fig. 5d), lean mass (Extended Data Fig. 5e), adipose tissue mass (Extended Data Fig. 5f, g), liver mass (Extended Data Fig. 5h), blood glucose (Extended Data Fig. 5i) or insulin levels (Extended Data Fig. 5j) in either genotype. mGIPR-Ab treatment reduced total plasma cholesterol in *Gipr*^{fl/fl} control mice but not in

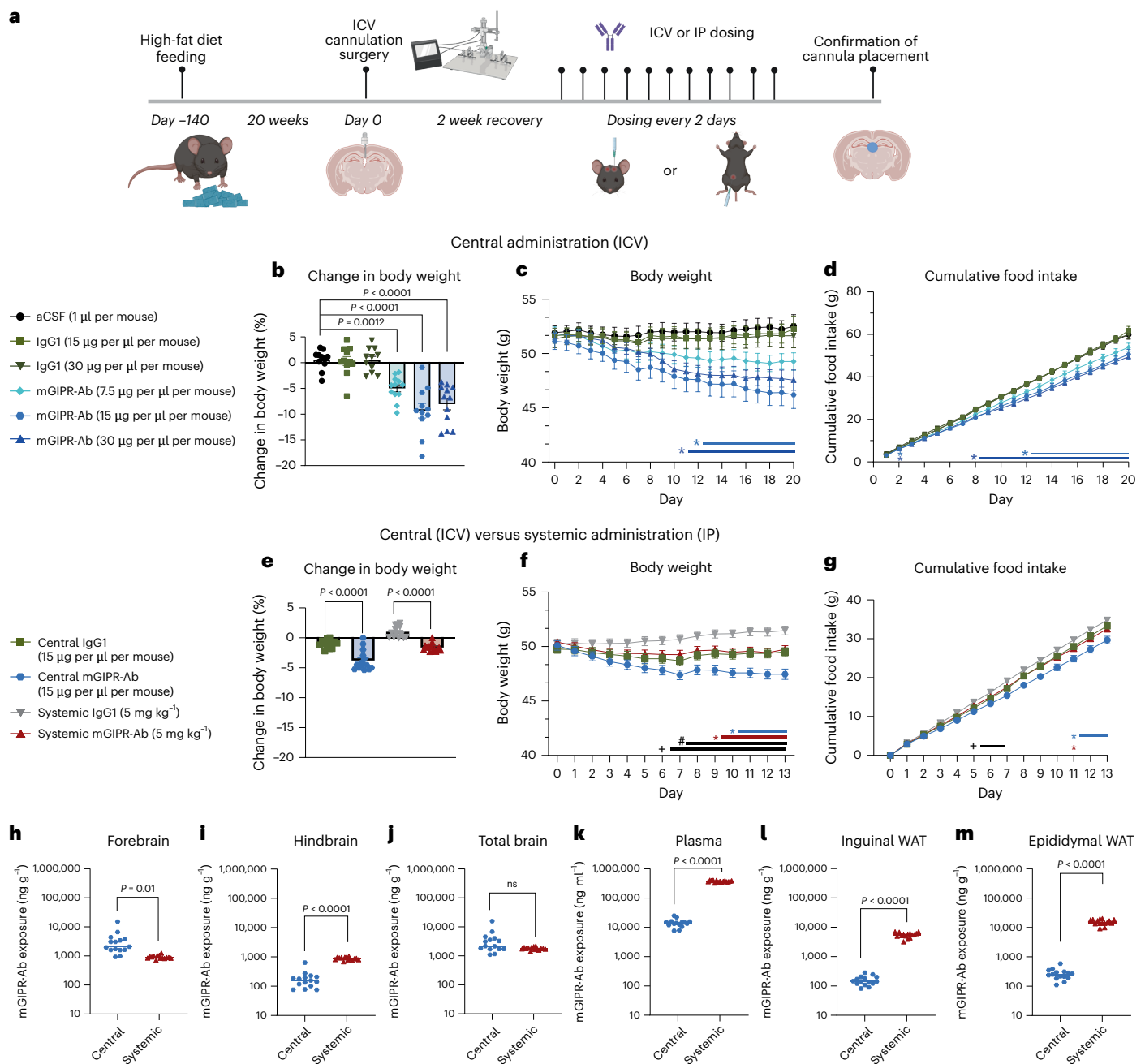


Fig. 1 | Anti-GIPR antibody administration to the brain reduces body weight and food intake in obese mice. a, Timeline of ICV and ICV versus IP dosing studies in obese mice (created with [BioRender.com](#)). To examine the dose response from central administration of mGIPR-Ab, male DIO mice received ICV cannula targeting the third ventricle in the brain. Mice were randomized into one of six groups: (1) vehicle/aCSF (1 μ l per mouse, $n = 11$), (2) IgG1 (15 μ g per μ l per mouse, $n = 11$), (3) IgG1 (30 μ g per μ l per mouse, $n = 11$), (4) mGIPR-Ab (7.5 μ g per μ l per mouse, $n = 12$), (5) mGIPR-Ab (15 μ g per μ l per mouse, $n = 11$) or (6) mGIPR-Ab (30 μ g per μ l per mouse, $n = 12$). All mice were dosed every 2 days for ten treatments. **b–d**, Change in body weight (**b**), body weight (**c**) and cumulative food intake (**d**) were measured daily. To directly compare central versus systemic administration of mGIPR-Ab, all male DIO mice received ICV cannula and were randomized into one of four groups: (1) central IgG1 (15 μ g per μ l per mouse), (2) central mGIPR-Ab (15 μ g per μ l per mouse), (3) systemic IgG1 (5 mg kg^{-1}) or (4) systemic mGIPR-Ab (5 mg kg^{-1}). All mice were dosed every 2 days for seven treatments. **e–g**, Change in body weight (**e**), body weight (**f**) and food intake (**g**) were measured daily. **h–m**, Pharmacokinetic exposure to mGIPR-Ab treatment

from central (ICV) and systemic (IP) dosing in forebrain (**h**), hindbrain (**i**), total brain (**j**), plasma (**k**), inguinal WAT (**l**) and epididymal WAT (**m**) was measured 48 h after the last dose. The forebrain and hindbrain were separated at around -3.87 mm from bregma. For **b,c**, aCSF (1 μ l per mouse, $n = 11$), IgG1 (15 μ g per μ l per mouse, $n = 11$), IgG1 (30 μ g per μ l per mouse, $n = 11$), mGIPR-Ab (7.5 μ g per μ l per mouse, $n = 12$), mGIPR-Ab (15 μ g per μ l per mouse, $n = 11$) and mGIPR-Ab (30 μ g per μ l per mouse, $n = 12$); for **d**, aCSF (1 μ l per mouse, $n = 9$), IgG1 (15 μ g per μ l per mouse, $n = 10$), IgG1 (30 μ g per μ l per mouse, $n = 11$), mGIPR-Ab (7.5 μ g per μ l per mouse, $n = 11$), mGIPR-Ab (15 μ g per μ l per mouse, $n = 8$) and mGIPR-Ab (30 μ g per μ l per mouse, $n = 12$); for **e–m**, $n = 15$ per group. In **b–g**, one-way or two-way repeated measures ANOVA with Tukey's test for multiple comparisons; in **h–m**, two-tailed unpaired t -test. * $P < 0.05$, ** $P < 0.01$, *** $P < 0.001$, **** $P < 0.0001$ versus aCSF (**b–d**) or versus IgG1 from respective dosing route or as noted by brackets (**e–g**); + $P < 0.05$, central IgG1 versus systemic IgG1; # $P < 0.05$, central mGIPR-Ab versus systemic mGIPR-Ab. Data represent means; error bars, s.e.m. aCSF, artificial cerebrospinal fluid.

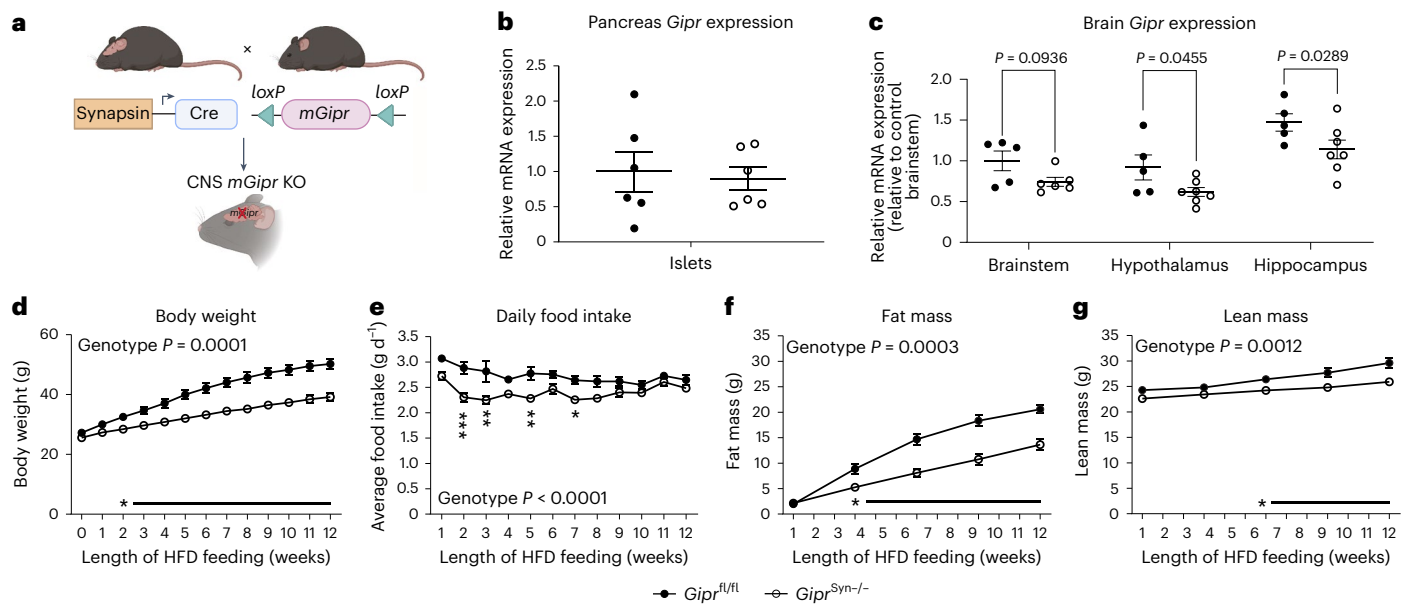


Fig. 2 | Mice with CNS KO of *Gipr* are resistant to diet-induced obesity. **a**, Breeding schematic for generation of CNS *Gipr* KO mice (created with BioRender.com). Male *Gipr^{fl/fl}* and *Gipr^{Syn-/-}* littermates were fed HFD for 12 weeks. **b,c**, *Gipr* RNA expression from isolated pancreatic islets (**b**) and brainstem, hypothalamus and hippocampus (**c**) were assessed to confirm CNS *Gipr* KO. **d**, Body weight, **e**, food intake, **f**, fat mass and **g**, lean mass were measured

throughout HFD feeding. For **b**, $n = 6$ mice per genotype; for **c**, *Gipr^{fl/fl}* ($n = 5$ per brain region), *Gipr^{Syn-/-}* ($n = 6$ brainstem, $n = 7$ hypothalamus and hippocampus); for **d–g**, *Gipr^{fl/fl}* ($n = 11$) and *Gipr^{Syn-/-}* ($n = 10$). In **b**, multiple unpaired *t*-tests with a 1% false discovery rate for multiple comparisons; in **c–f**, two-way ANOVA with Sidák's test for multiple comparisons. * $P < 0.05$, ** $P < 0.01$, *** $P < 0.001$, **** $P < 0.0001$. Data represent mean; error bars, s.e.m.

Gipr^{Syn-/-} mice. However, *Gipr^{Syn-/-}* mice had reduced total plasma cholesterol, regardless of treatment, compared to vehicle-treated *Gipr^{fl/fl}* control mice (Extended Data Fig. 5k). These findings demonstrate that *Gipr^{Syn-/-}* mice are resistant to the weight-lowering effects of mGIPR-Ab, highlighting the crucial role of CNS GIPR for the body weight response to mGIPR-Ab.

Loss of CNS GIPR augments weight loss with GLP-1R agonism

To examine whether CNS GIPR is required for the additive weight loss effect of combination treatment with mGIPR-Ab and clinically approved GLP-1R agonists, HFD-fed *Gipr^{fl/fl}* control mice and *Gipr^{Syn-/-}* mice received IP dosing of either vehicle–vehicle, dulaglutide–vehicle or dulaglutide–mGIPR-Ab combination treatments. In *Gipr^{fl/fl}* mice, dulaglutide–vehicle treatment resulted in significant reductions in body weight compared to vehicle–vehicle treatment (Fig. 3a,b). Moreover, dulaglutide–mGIPR-Ab treatment resulted in significantly more body weight loss than with the dulaglutide–vehicle treatment (Fig. 3a,b). Interestingly, dulaglutide alone produced even greater weight loss in *Gipr^{Syn-/-}* mice; however, the potentiating effect of simultaneous GIPR antagonism and GLP-1R agonism evident in *Gipr^{fl/fl}* control mice was absent in *Gipr^{Syn-/-}* mice (Fig. 3a,c). These data demonstrate that the mGIPR-Ab extends the weight loss of GLP-1R agonist treatment. Moreover, loss of CNS *Gipr* expression potentiates the actions of dulaglutide yet abrogates the additional benefit of combining GIPR blockade with GLP-1R agonism. The blunted effect of combined therapy in *Gipr^{Syn-/-}* mice was also observed with food intake (Fig. 3d,e) and fat mass (Fig. 3f), but not inguinal (Fig. 3g) and epididymal (Fig. 3h) WAT weights. Additionally, the treatment effects of combined dulaglutide–mGIPR-Ab were absent in liver weight (Fig. 3i), blood glucose (Fig. 3j) and insulin in *Gipr^{Syn-/-}* mice (Fig. 3k), in part reflecting lower baseline values for these parameters in *Gipr^{Syn-/-}* mice.

CNS GIPR and GLP-1R are essential for maximal weight loss

To interrogate the importance of CNS GIPR for weight loss with mGIPR-Ab/GLP-1 treatment, HFD-fed *Gipr^{fl/fl}* and *Gipr^{Syn-/-}* mice were treated IP with either vehicle or mGIPR-Ab/P1 every 6 days for 18 days.

Vehicle-treated *Gipr^{fl/fl}* and *Gipr^{Syn-/-}* mice showed a 1.5% and 2.6% weight gain, respectively, whereas mGIPR-Ab/P1-treated *Gipr^{fl/fl}* mice lost 20% of their body weight (Fig. 4a–c). By contrast, mGIPR-Ab/P1-treated *Gipr^{Syn-/-}* mice only lost 12% of their body weight despite preservation of intact GLP-1R signalling (Fig. 4a–c), revealing the essential role of CNS GIPR for the maximal weight loss response to combined GIPR blockade/GLP-1R activation. *Gipr^{fl/fl}* and *Gipr^{Syn-/-}* mice treated with mGIPR-Ab/P1 exhibited lower food intake (Fig. 4d), lower total fat (Fig. 4e), inguinal WAT (Fig. 4f), epididymal WAT (Fig. 4g) and liver (Fig. 4h) weights compared to vehicle-treated mice; these parameters were often lower at baseline and did not change following mGIPR-Ab/P1 treatment in *Gipr^{Syn-/-}* mice.

We next examined whether CNS GLP-1R is also essential for the full weight loss effects of mGIPR-Ab/P1 treatment. *Wnt1* was used to drive Cre expression in *Glp1r^{fl/fl}* mice to generate CNS GLP-1R KO mice (Fig. 5a), as this model has been thoroughly characterized^{19,20}. Male HFD-fed *Glp1r^{fl/fl}* control mice and *Glp1r^{Wnt1-/-}* mice were treated IP with either vehicle or mGIPR-Ab/P1 every 6 days for 18 days. On day 18, vehicle-treated *Glp1r^{fl/fl}* and *Glp1r^{Wnt1-/-}* male mice maintained stable body weight, losing only 0.8–1.3% of their initial weight (Fig. 5b–d). *Glp1r^{fl/fl}* mice treated with mGIPR-Ab/P1 lost 16% of their body weight, whereas the extent of weight loss (9%) was diminished in mGIPR-Ab/P1-treated *Glp1r^{Wnt1-/-}* mice (Fig. 5b–d). These data indicate that the weight loss effects of the mGIPR-Ab/GLP-1 peptide–antibody conjugate are not exclusively driven by GLP-1R agonism. The blunted weight loss in mGIPR-Ab/P1-treated *Glp1r^{Wnt1-/-}* mice was associated with less reduction in food intake compared to *Glp1r^{fl/fl}* controls (Fig. 5e). *Glp1r^{fl/fl}* mice treated with mGIPR-Ab/P1 also had lower total fat and inguinal WAT weights compared to vehicle, whereas *Glp1r^{Wnt1-/-}* mice treated with mGIPR-Ab/P1 showed no significant differences (Fig. 5f,g). The mGIPR-Ab/P1 treatment did not reduce epididymal weight (Fig. 5h) or liver weight (Fig. 5i) in either the *Glp1r^{fl/fl}* or *Glp1r^{Wnt1-/-}* mice.

To investigate whether the metabolic effects of mGIPR-Ab/GLP-1 are similar in female mice, we treated female HFD-fed *Glp1r^{fl/fl}* control and *Glp1r^{Wnt1-/-}* mice with IP injection of either vehicle or mGIPR-Ab/P1 every 6 days for 18 days. Similar to findings in male

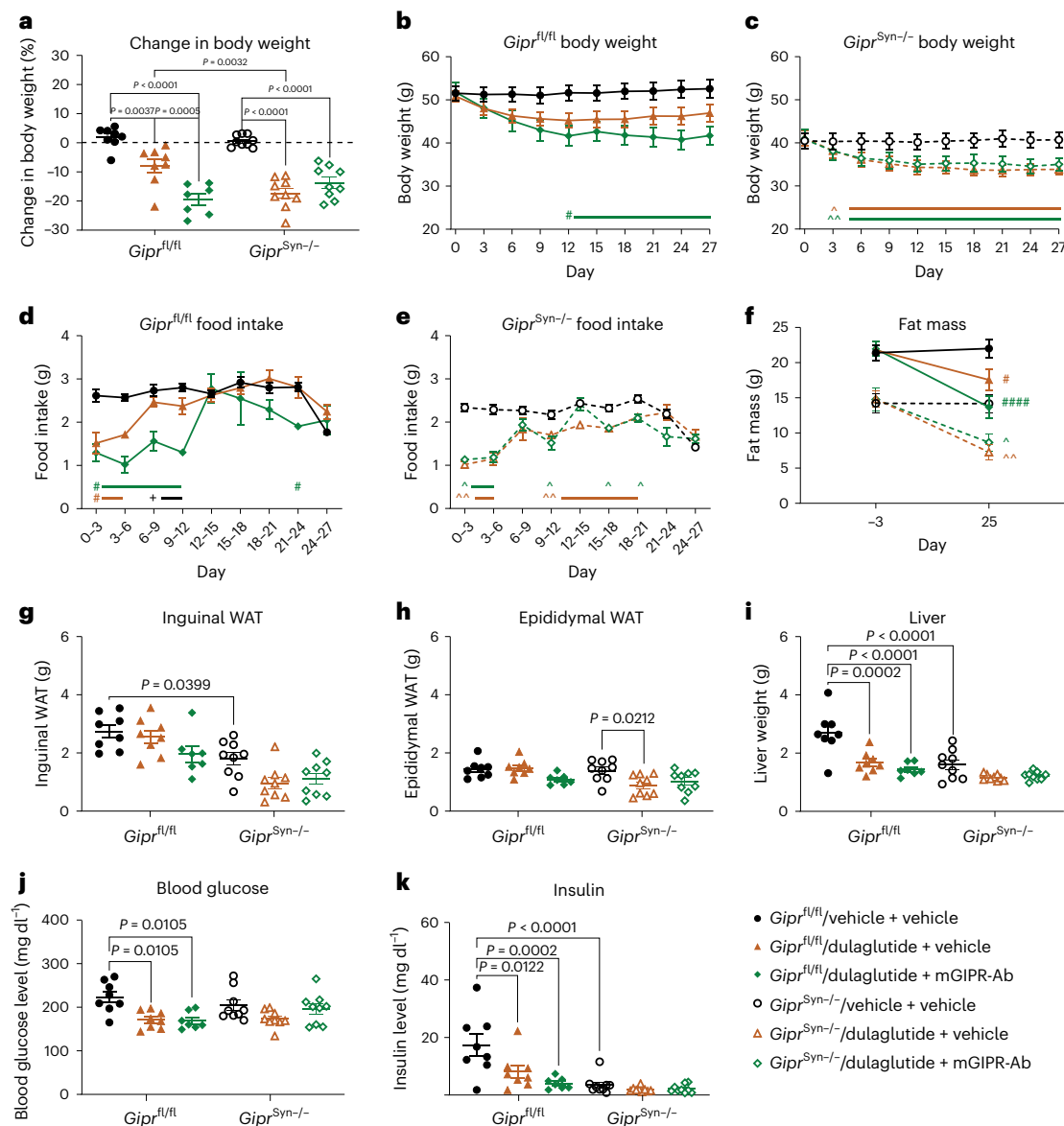


Fig. 3 | *Gipr* KO in the CNS extends the body weight reduction and anorectic effect of GLP-1R agonism in DIO mice. Male *Gipr*^{fl/fl} and *Gipr*^{Syn-/-} littermates were fed HFD for 14 weeks and then treated IP with vehicle (2 ml kg⁻¹ every 3 days) + vehicle (2 ml kg⁻¹ every 6 days), dulaglutide (0.3 mg kg⁻¹ every 3 days) + vehicle (2 ml kg⁻¹ every 6 days) or dulaglutide (0.3 mg kg⁻¹ every 3 days) + mGIPR-Ab (25 mg kg⁻¹ every 6 days) for 27 days (all mice received the same number of injections each dosing day). **a**, Day 27 body weight per cent change. **b–e**, Body weight over time in *Gipr*^{fl/fl} (**b**) and *Gipr*^{Syn-/-} (**c**) littermates and average daily food intake measured every 3 days in *Gipr*^{fl/fl} (**d**) and *Gipr*^{Syn-/-} (**e**) littermates. **f**, Fat mass measured by MRI on days -3 and 25. **g–i**, Day 27 necropsy tissue weights inguinal of WAT (**g**), epididymal WAT (**h**) and liver (**i**). **j, k**, Day 27 4 h fasted blood glucose (**j**) and plasma insulin (**k**). For **a–k**, *Gipr*^{fl/fl} / vehicle + vehicle

(*n* = 8) *Gipr*^{fl/fl} / dulaglutide + vehicle (*n* = 8), *Gipr*^{fl/fl} / dulaglutide + mGIPR-Ab (*n* = 7), *Gipr*^{Syn-/-} / vehicle + vehicle (*n* = 9), *Gipr*^{Syn-/-} / dulaglutide + vehicle (*n* = 9), *Gipr*^{Syn-/-} / dulaglutide + mGIPR-Ab (*n* = 9). In **a–c** and **f–k**, one-way or two-way repeated measures ANOVA with Tukey's test for multiple comparisons; in **d** and **e**, mixed-effects analysis with genotype and treatment as main factors followed by Tukey's test for multiple comparisons. **P* < 0.05, ***P* < 0.01, ****P* < 0.001, *****P* < 0.0001 versus vehicle + vehicle within genotype or comparison indicated by brackets; #*P* < 0.05, ##*P* < 0.01 versus vehicle + vehicle within genotype (*Gipr*^{fl/fl}); ^*P* < 0.05, ^^*P* < 0.01 versus vehicle + vehicle within genotype (*Gipr*^{Syn-/-}); +*P* < 0.05, *Gipr*^{fl/fl} / dulaglutide + vehicle versus *Gipr*^{fl/fl} / dulaglutide + mGIPR-Ab. Data represent means; error bars, s.e.m. MRI, magnetic resonance imaging.

mice, vehicle-treated *Glp1r*^{fl/fl} and *Glp1r*^{Wnt1-/-} mice showed weight gain or maintenance of body weight, changing by 4.6% and -0.4%, respectively, over the course of treatment. Meanwhile, female *Glp1r*^{fl/fl} mice treated with mGIPR-Ab/P1 lost 19.4% of their body weight; however, weight loss (8.1%) was markedly attenuated in female *Glp1r*^{Wnt1-/-} mice treated with mGIPR-Ab/P1 (Fig. 5j–l). mGIPR-Ab/P1 treatment did not produce differences in fat mass (Fig. 5m), inguinal WAT (Fig. 5n), gonadal WAT (Fig. 5o) or liver weight (Fig. 5p) for either genotype in female mice.

Liver and WAT transcriptomic analyses

To examine downstream systemic effects of genetic and pharmacologic manipulations, transcriptomic analysis was conducted on inguinal WAT (Fig. 6) and liver (Extended Data Fig. 6) from *Gipr*^{fl/fl}, *Gipr*^{Syn-/-}, *Glp1r*^{fl/fl} and *Glp1r*^{Wnt1-/-} mice treated with either vehicle or mGIPR-Ab/P1. Interestingly, transcriptomic changes were evident in both inguinal WAT and liver from vehicle-treated *Gipr*^{Syn-/-} mice (Fig. 6a,b and Extended Data Fig. 6a,b). These changes were similar to those observed in *Gipr*^{fl/fl} (Fig. 6a,b and Extended Data Fig. 6a,b) and *Glp1r*^{fl/fl} mice (Fig. 6c,d and Extended Data

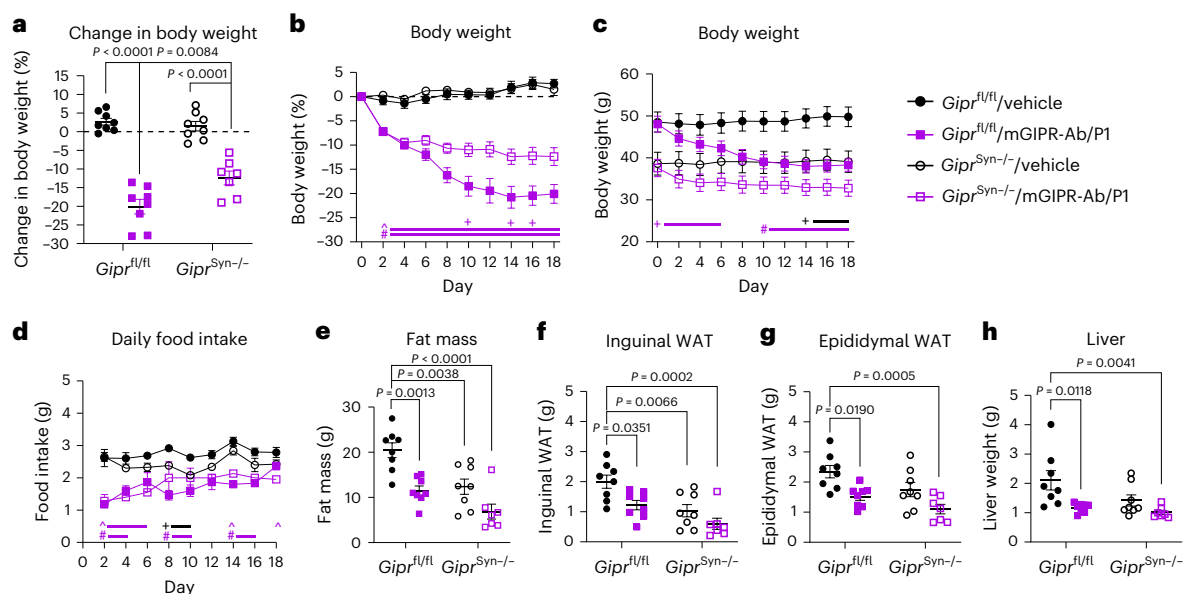


Fig. 4 | Weight loss pursuant to treatment with the mGIPR-Ab/GLP-1 peptide-antibody conjugate requires GIPR activity in the CNS. Male *Gipr*^{fl/fl} and *Gipr*^{Syn-/-} littermates were fed HFD for 13 weeks and then treated with vehicle (2 ml kg⁻¹ every 6 days) or mGIPR-Ab/P1 (1.5 mg kg⁻¹ every 6 days) for 18 days. **a**, Day 18 body weight per cent change, **b**, per cent body weight change from day 0 and **c**, change in body weight over time in *Gipr*^{fl/fl} and *Gipr*^{Syn-/-} littermates. **d**, Average daily food intake in *Gipr*^{fl/fl} and *Gipr*^{Syn-/-} littermates. **e**, Fat mass measured by MRI on day 17. **f**, Day 18 necropsy tissue weights for inguinal WAT, **g**, epididymal WAT and **h**, liver. For **a–h**, *Gipr*^{fl/fl} / vehicle (*n* = 8), *Gipr*^{fl/fl} / mGIPR-Ab/P1 (*n* = 8),

Gipr^{Syn-/-} / vehicle (*n* = 8), *Gipr*^{Syn-/-} / mGIPR-Ab/P1 (*n* = 7). In **a** and **e–h**, two-way ANOVA with Tukey's multiple comparisons test; **b–d**, two-way repeated measures ANOVA or mixed-effects analysis with genotype and treatment as main factors followed by a Tukey's test for multiple comparisons. **P* < 0.05, ***P* < 0.01, ****P* < 0.001, *****P* < 0.0001 vs vehicle within genotype or comparison indicated by bracket; # indicates *P* < 0.05 versus vehicle within genotype (*Gipr*^{fl/fl}), ^ indicates *P* < 0.05 versus vehicle within genotype (*Gipr*^{Syn-/-}), + (purple) indicates *P* < 0.05 versus *Gipr*^{fl/fl} within mGIPR-Ab/P1 treatment, + (black) indicates *P* < 0.05 versus *Gipr*^{fl/fl} within vehicle treatment. Data represent means; error bars, s.e.m.

Fig. 6c,d) treated with mGIPR-Ab/P1. In inguinal WAT, direct comparison between *Gipr*^{fl/fl} vehicle-treated and *Gipr*^{fl/fl} mGIPR-Ab/P1-treated mice resulted in 1,118 differentially expressed genes (DEGs) with 450 upregulated and 668 downregulated genes. Similarly, in WAT, a direct comparison between *Gipr*^{fl/fl} vehicle and *Gipr*^{Syn-/-} vehicle groups resulted in 1,856 DEGs with 909 upregulated and 947 downregulated genes. Ingenuity Pathway Analysis showed that compared to vehicle treatment, mGIPR-Ab/P1 treatment of *Gipr*^{fl/fl} and *Gipr*^{Syn-/-} mice resulted in negative enrichment in cell cycle regulation, cholesterol biosynthesis, extracellular matrix (ECM) and collagen organization, and immune response and inflammation pathways in both WAT and liver (Fig. 6a,c and Extended Data Fig. 6a,c). Likewise, comparison between *Gipr*^{fl/fl} vehicle-treated and *Gipr*^{Syn-/-} vehicle-treated groups demonstrated negative enrichment in cholesterol biosynthesis, ECM and collagen organization, and immune response and inflammation pathways (Fig. 6a and Extended Data Fig. 6a). By contrast, when comparing *Gipr*^{fl/fl} vehicle-treated mice to *Gipr*^{Syn-/-} vehicle-treated mice, there were no observed DEGs in inguinal WAT or liver (Fig. 6c,d and Extended Data Fig. 6c,d).

Genes from the three or four most significantly enriched pathways from all comparisons were ranked according to *P* value (adjusted) and subsequently displayed on a heatmap with log(fold change) represented by colour. Pathways enriched for DEGs selected from *Gipr*^{fl/fl} vehicle versus *Gipr*^{Syn-/-} vehicle, as well as *Gipr*^{fl/fl} vehicle versus *Gipr*^{fl/fl} mGIPR-Ab/P1 comparisons, demonstrated that reduction of CNS GIPR function through either pharmacological or genetic intervention led to downregulation within adipose tissue of key canonical genes within these pathways (Fig. 6b and Extended Data Fig. 6b). In the cholesterol biosynthesis pathway, expression of genes such as lanosterol synthase (*Lss*), cytochrome P450, family 51 (*Cyp51*), NAD(P) dependent steroid dehydrogenase-like (*Nsdhl*) and 7-dehydrocholesterol reductase (*Dhcr7*) were decreased. Similarly, genes involved in cell cycle regulation and ECM organization, including those in the collagen biosynthesis and modifying enzymes pathway (ADAM metalloproteinase

domain 12 (*Adam12*), laminin subunit beta 3 (*Lamb3*), collagen type VI alpha 3 (*Col6a3*), neurocan (*Ncan*) and integrin alpha 6 (*Itga6*) also exhibited reduced expression. Additionally, comparison between *Gipr*^{fl/fl} vehicle and *Gipr*^{Syn-/-} vehicle groups revealed that reduced CNS GIPR function led to an overall decrease in gene expression related to immune response and inflammation, particularly within the neutrophil degranulation pathway, where serine peptidase inhibitor, clade A, member 3 M (*Serpina3m*), deoxyribose-phosphate aldolase (*Dera*), fatty acid binding protein 5 (*Fabp5*), ATP citrate lyase (*Acl*) and cathepsin D (*Ctsd*) were downregulated.

Systemic mGIPR-Ab/GLP-1 activates brain regions involved in food intake control

To determine whether mGIPR-Ab/GLP-1 peptide-antibody conjugates access brain regions expressing GIPR and GLP-1R, IgG1 immunostaining was used to visualize mGIPR-Ab/P3 biodistribution in the brain 4 h after IP administration. mGIPR-Ab/P3 was detected in circumventricular organs (CVOs) in the brain, including the vascular organ of the lamina terminalis, subfornical organ, median eminence and area postrema (AP) (Fig. 7a). Biodistribution was consistent across mice and significant in comparison to mice treated with vehicle (Fig. 7b,c). We next determined c-Fos expression to assess neuronal activation induced by mGIPR-Ab/GLP-1. Despite localization of mGIPR-Ab/P3 predominantly in CVOs, and not in deeper parenchyma of the brain, c-Fos activation was observed in multiple neural substrates involved in food intake control^{21–30} (Fig. 7d–f). Regions with significantly greater c-Fos activation included the bed nuclei of the stria terminalis, paraventricular thalamus, central amygdalar nucleus (Fig. 7g), paraventricular nucleus, parabrachial nucleus (Fig. 7h), nucleus of the solitary tract (Fig. 7i), dorsal motor nucleus of the vagus nerve and AP. Interestingly, many of these brain regions do not express *Gipr* or *Glp1r*^{31,32}, suggesting that these are secondary downstream pathways that are activated indirectly by mGIPR-Ab/P3.

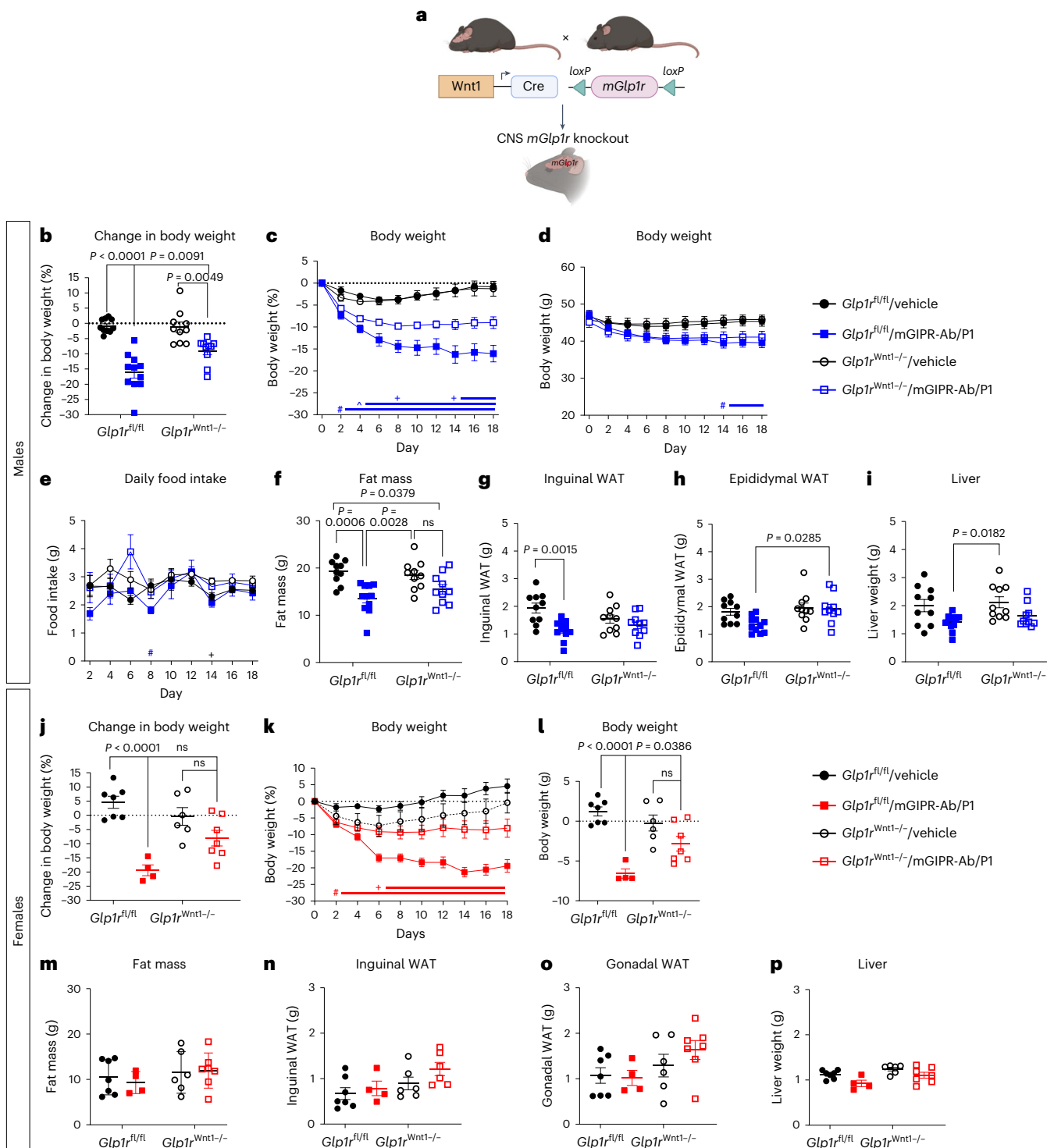


Fig. 5 | Weight loss generated by the mGIPR-Ab/GLP-1 peptide-antibody conjugate is dependent on GLP-1R activity in the CNS. **a**, Breeding schematic for generation of CNS *Glp1r* KO mice (created with BioRender.com). Male (blue) and female (red) *Glp1^{fl/fl}* and *Glp1^{Wnt1-/-}* littermates were fed HFD for 13 weeks and then treated with vehicle (2 ml kg⁻¹ every 6 days) or mGIPR-Ab/P1 (1.5 mg kg⁻¹ every 6 days) for 18 days. **b, j**, Day 18 body weight per cent change, **c, k**, per cent body weight change from day 0 and **d, l**, change in body weight over time in male and female *Glp1^{fl/fl}* and *Glp1^{Wnt1-/-}* littermates. **e**, Average daily food intake in male *Glp1^{fl/fl}* and *Glp1^{Wnt1-/-}* littermates. **f, m**, Fat mass measured by MRI on day 17. **g, n**, Inguinal WAT, **h, o**, gonadal WAT and **i, p**, liver. For **b–i** (males), *Glp1^{fl/fl}* / vehicle (*n* = 10), *Glp1^{fl/fl}* / mGIPR-Ab/P1 (*n* = 11), *Glp1^{Wnt1-/-}* / vehicle (*n* = 10) and *Glp1^{Wnt1-/-}* / mGIPR-Ab/P1 (*n* = 10). For **j–p** (females), *Glp1^{fl/fl}* / vehicle (*n* = 7), *Glp1^{fl/fl}* / mGIPR-Ab/P1 (*n* = 4), *Glp1^{Wnt1-/-}* / vehicle (*n* = 6) and *Glp1^{Wnt1-/-}* / mGIPR-Ab/P1 (*n* = 7). In **b, f–i, j** and **l–o**, two-way ANOVA with Tukey's multiple comparisons test; in **c–e** and **k**, two-way repeated measures ANOVA with genotype and treatment as main factors or mixed-effects analysis followed by a Tukey's multiple comparisons test. **P* < 0.05, ***P* < 0.01, ****P* < 0.001, *****P* < 0.0001 where comparison indicated by bracket; # indicates *P* < 0.05 versus vehicle within genotype (*Glp1^{fl/fl}*), ^ indicates *P* < 0.05 versus vehicle within genotype (*Glp1^{Wnt1-/-}*), + (blue or red) indicates *P* < 0.05 versus *Glp1^{fl/fl}* within mGIPR-Ab/P1 treatment, + (black) indicates *P* < 0.05 versus *Glp1^{fl/fl}* within vehicle treatment. Data represent means; error bars, s.e.m. ns, not significant.

Day 18 necropsy tissue weights for **g, n** inguinal WAT, **h, o**, gonadal WAT and **i, p**, liver. For **b–i** (males), *Glp1^{fl/fl}* / vehicle (*n* = 10), *Glp1^{fl/fl}* / mGIPR-Ab/P1 (*n* = 11), *Glp1^{Wnt1-/-}* / vehicle (*n* = 10) and *Glp1^{Wnt1-/-}* / mGIPR-Ab/P1 (*n* = 10). For **j–p** (females), *Glp1^{fl/fl}* / vehicle (*n* = 7), *Glp1^{fl/fl}* / mGIPR-Ab/P1 (*n* = 4), *Glp1^{Wnt1-/-}* / vehicle (*n* = 6) and *Glp1^{Wnt1-/-}* / mGIPR-Ab/P1 (*n* = 7). In **b, f–i, j** and **l–o**, two-way ANOVA with Tukey's multiple comparisons test; in **c–e** and **k**, two-way repeated measures ANOVA with genotype and treatment as main factors or mixed-effects analysis followed by a Tukey's multiple comparisons test. **P* < 0.05, ***P* < 0.01, ****P* < 0.001, *****P* < 0.0001 where comparison indicated by bracket; # indicates *P* < 0.05 versus vehicle within genotype (*Glp1^{fl/fl}*), ^ indicates *P* < 0.05 versus vehicle within genotype (*Glp1^{Wnt1-/-}*), + (blue or red) indicates *P* < 0.05 versus *Glp1^{fl/fl}* within mGIPR-Ab/P1 treatment, + (black) indicates *P* < 0.05 versus *Glp1^{fl/fl}* within vehicle treatment. Data represent means; error bars, s.e.m. ns, not significant.

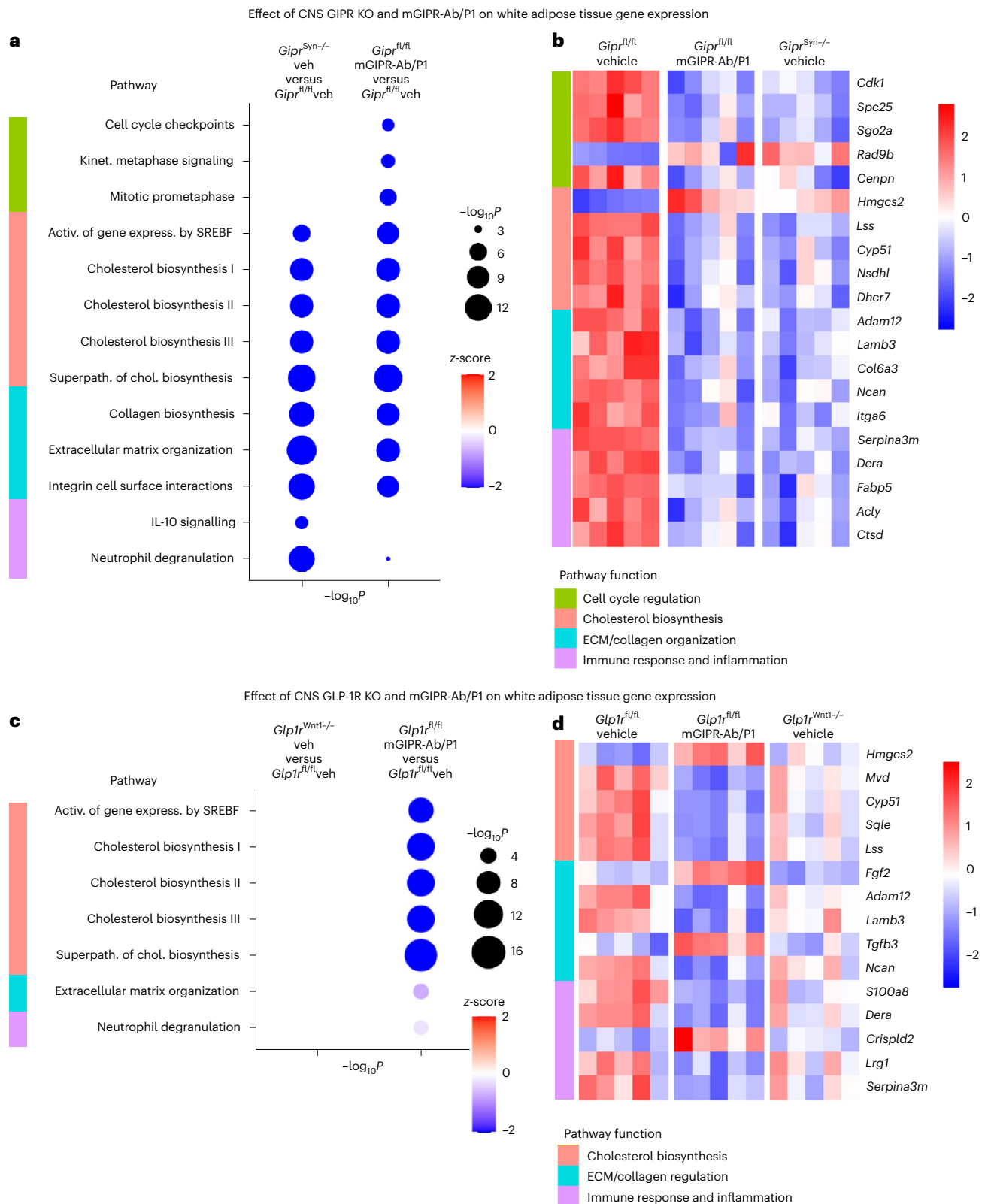


Fig. 6 | mGIPR-Ab/P1 peptide-antibody conjugate treatment and CNS GIPR KO result in gene expression profile changes in WAT. Transcriptomic analysis was conducted on WAT from male DIO *Gipr^{fl/fl}*, *Gipr^{Syn-/-}*, *Glp1r^{fl/fl}* and *Glp1r^{Wnt1-/-}* mice treated with either vehicle or mGIPR-Ab/P1. Samples were analysed for differential gene expression using DESeq2, and Ingenuity Pathway Analysis was used to identify the most significantly affected pathways. **a,c**, Bubble plot representing pathways enriched for DEGs in *Gipr^{Syn-/-}* vehicle-treated and *Gipr^{fl/fl}* mGIPR-Ab/P1-treated mice (**a**), and *Glp1r^{Wnt1-/-}* vehicle-treated and *Glp1r^{fl/fl}*

mGIPR-Ab/P1-treated mice (**c**). Bubble size represents P value and colour shade represents z-score/enrichment score for each pathway. **b,d**, Heatmap for top five genes per enriched pathway in *Gipr^{Syn-/-}* vehicle-treated and *Gipr^{fl/fl}* mGIPR-Ab/P1-treated mice (**b**) and *Glp1r^{Wnt1-/-}* vehicle-treated and *Glp1r^{fl/fl}* mGIPR-Ab/P1-treated mice (**d**). Top five genes were selected based on biological relevance and statistical significance. In **a** and **c**, right-tailed Fisher's exact test; $n = 5$ per group. Activ. of gene express., activation of gene expression; ECM, extracellular matrix; superpath., superpathway; veh, vehicle.

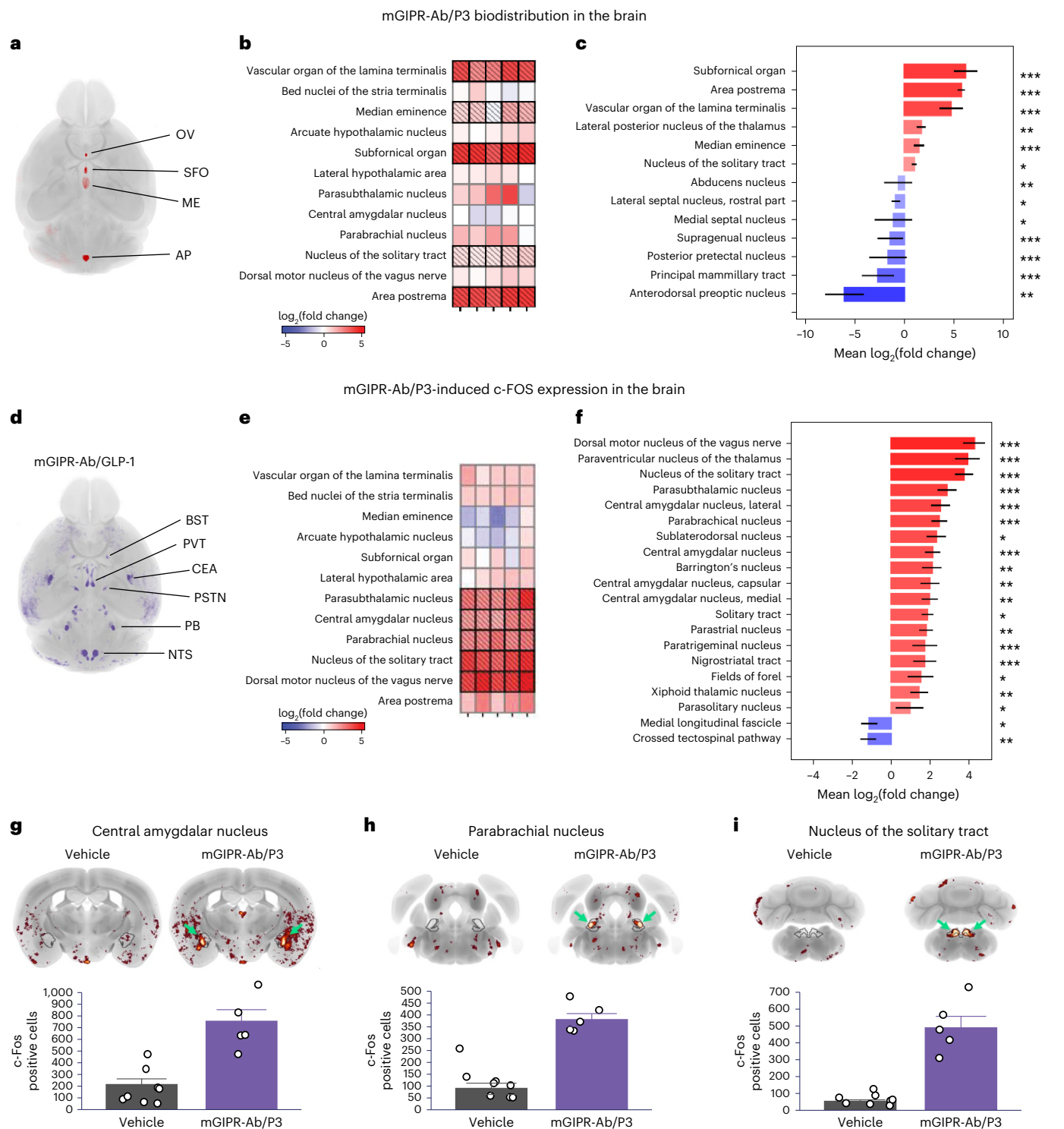


Fig. 7 | mGIPR-Ab/P3 peptide–antibody conjugate is measurable in CVOs in the brain and induces c-Fos in the central nucleus of the amygdala, parabrachial nucleus and nucleus of the solitary tract. DIO male mice were treated with vehicle or mGIPR-Ab/P3 4 h before IgG1 measurement and c-FOS analysis. **a**, Horizontal cross-section of brain showing IgG1, a marker for mGIPR-Ab/GLP-1 peptide–antibody conjugate, biodistribution in vascular organ of the lamina terminalis, subfornical organ, median eminence and AP. **b**, Heatmap showing $\log_2(\text{fold change})$ in IgG1 across five mice. **c**, Bar chart demonstrating brain regions significantly greater $\log_2(\text{fold change})$ in average IgG1 staining in mGIPR-Ab/P3 group than in average vehicle, ranked by P value. **d**, Horizontal cross-section of brain showing group average c-Fos activity signature in response to mGIPR-Ab/P3 compared with vehicle. Scale bar, 500 μm . **e**, Heatmap showing $\log_2(\text{fold change})$ in c-Fos following mGIPR-Ab/P3 treatment across five mice.

f, Bar chart demonstrating brain regions significantly greater fold change in average mGIPR-Ab/P3 group in comparison to average vehicle, ranked by P value. **g–i**, Representative c-Fos activity in the central amygdalar nucleus (**g**), parabrachial nucleus (**h**) and nucleus of the solitary tract (**i**) in vehicle or mGIPR-Ab/P3 treated group. For **a–i**, vehicle ($n = 8$) and mGIPR-Ab/P3 ($n = 5$); in **c** and **f–i**, negative binomial generalized linear model, followed by Dunnett's test for multiple comparisons. $^*P < 0.05$, $^{**}P < 0.01$, $^{***}P < 0.001$ compared to vehicle. Data represent means; error bars, s.e.m. AP, area postrema; BST, bed nuclei of the stria terminalis; CEA, central amygdalar nucleus; CVO, circumventricular organs; DIO, diet-induced obese; ME, median eminence; NTS, nucleus of the solitary tract; OV, vascular organ of the lamina terminalis; PB, parabrachial nucleus; PSTN, parasubthalamic nucleus; PVT, paraventricular nucleus of the thalamus; SFO, subfornical organ.

Given that the mGIPR-Ab/GLP-1 peptide–antibody conjugate probably accesses the brain through CVOs, with the highest concentration in the AP, *Gipr* and *Glp1r* mRNA were measured in the mouse AP. *Gipr* and *Glp1r* mRNA were detected on different cells in the AP and semi-quantitatively scored at level two (four to nine dots per cell, few or no clusters) using Advanced Cell Diagnostics criteria (Extended Data Fig. 7a). This suggests that the mGIPR-Ab/GLP-1 peptide–antibody conjugate may be able to directly act on GIPR and GLP-1R in the AP to trigger c-Fos activation in the brain. To assess the effect of GIPR antagonism on GIP-induced c-Fos activation in the AP, mice were pre-treated with IP IgG1, mGIPR-Ab or mGIPR-Ab/P3, followed 24 h later by IP vehicle or [D-Ala²]-GIP (DA-GIP; 0.5 mg kg⁻¹). Brains were dissected 4 h later, and c-Fos expression was assessed. Mice pre-treated with IgG1 and then DA-GIP show significantly more c-Fos⁺ cells in the AP compared to mice pre-treated with IgG1 and then vehicle (Extended Data Fig. 7b,e). This effect was 80.7% reduced in mice pre-treated with mGIPR-Ab (Extended Data Fig. 7c,e). Interestingly, mice pre-treated with mGIPR-Ab/P3 followed by vehicle show increased c-Fos activation in the AP but a non-significant decrease in c-Fos⁺ cells when followed by DA-GIP treatment (Extended Data Fig. 7d,e). These results suggest that the mGIPR-Ab and GLP-1 components of the peptide–antibody conjugate target and differentially modulate activation of different cell subpopulations in the AP.

Discussion

Here, we further interrogated the mechanisms linking mGIPR-Ab/GLP-1 peptide–antibody conjugates to weight loss and improved metabolic markers in preclinical and clinical studies^{15–17}. Characterizing the biological mechanism(s) by which these molecules achieve weight loss remains a key question in understanding and improving therapeutics for the treatment of obesity. We demonstrate that mGIPR-Ab/GLP-1 peptide–antibody conjugates act on CNS GIP and GLP-1 receptors via CVOs to activate neural pathways, enabling the reduction of food intake and weight loss in obese mice.

Notably, CNS GIPR antagonism produces body weight loss in obese mice and also extends the anorectic effect of a GLP-1R agonist. We used an mGIPR-Ab that fully neutralizes GIPR activity in vitro and prevents body weight gain in obese mice when dosed systemically¹⁷. When administered directly to the brain, mGIPR-Ab effectively reduces body weight and food intake. These data align with previous work³³ that also demonstrated that central administration of a GIPR antagonist antibody (Gipg013) has anti-obesity effects in DIO mice and leads to decreased hypothalamic expression of suppressor of cytokine signalling 3 (*Socs3*), an inhibitor of leptin. Intriguingly, both acute and chronic central administration of GIP also results in body weight reduction in mice and rats^{34,35}. Moreover, central administration of GIP upregulates hypothalamic mRNA expression of genes regulating food intake and metabolism, including arginine vasopressin (*Avp*), cocaine and amphetamine regulated transcripts (*Cart*), cAMP responsive element binding protein 1 (*Creb1*), gamma-aminobutyric acid A receptor, subunit delta (*Gabrd*), janus kinase 2 (*Jak2*), mitogen-activated protein kinase 1 (*Mapk1*), neuropeptide Y (*Npy*), oxytocin (*Oxt*), signal transducer and activator of transcription 3 (*Stat3*) and tyrosine hydroxylase (*Th*), which is not observed in whole-body GIPR KO mice³⁵. These results suggest that GIPR activation in the CNS also interacts with anorexigenic signals to reduce body weight and food intake. One possible explanation for the similar effects on weight loss observed with both GIPR agonism and antagonism might be that chronic pharmacological GIPR activation induces functional antagonism in a subset of neurons through receptor desensitization, as seen in adipocytes, isolated pancreatic islets and mouse neuroblastoma Neuro2a cells^{36,37}. A recent study found that certain GIPR genetic variants that impair both Gs and beta-arrestin 2 recruitment are linked to lower adiposity³⁸, suggesting that GIPR effects on body weight involve complex signalling pathways. Additionally, it has been suggested that GIPR agonists and antagonists

might target different CNS receptor populations, with evidence showing that acylated peptide GIPR agonists act on GABAergic neurons to further reduce food intake and body weight when combined with GLP-1R agonists in mice^{39,40}. Further work is necessary to characterize the differences between GIPR agonism and antagonism and their impact on these molecular signalling pathways in the CNS.

In addition to the neuropharmacological effects of GIPR antagonism, we also demonstrate that CNS GIPR KO prevents body weight gain under HFD challenge, supporting the role of CNS GIPR as a primary driver of body weight differences seen in the whole-body GIPR KO mouse⁴¹. Previous work also demonstrated that CNS GIPR KO mice, generated using nestin-Cre, are protected from DIO and glucose intolerance¹⁸. Studies using single-cell RNA-sequencing show that *Gipr* is expressed in various cell types, including neurons, oligodendrocytes, mesenchymal cells and pericyte and tanycyte mural cells^{10–12}. Nestin is found in several cell subsets, such as neural stem and progenitor cells, glia, mesenchymal stromal cells, endothelial cells and Schwann cell precursors in the peripheral nervous system⁴². By contrast, synapsin-Cre enables more neuron-selective *Gipr* deletion. Although both approaches support the role of CNS GIPR in energy balance, the current experiments targeting the neuronal *Gipr* further pinpoint the specific cell types involved in body weight regulation. We also expand on these findings by showing that KO of CNS GIPR can sensitize the response to GLP-1R agonism and that CNS GIPR is necessary for the maximal weight loss response to mGIPR-Ab/GLP-1. Future work is necessary to understand the mechanisms and signalling pathways downstream of GIPR in neurons. Collectively, these data support that CNS GIPR signalling has an important role in regulating energy metabolism and is an important target for anti-obesity medications.

Given the role of CNS GIPR in energy balance and the impact of GIPR antagonism on body weight, it had been unclear whether mGIPR-Ab/GLP-1 peptide–antibody conjugates target GLP-1R predominantly or also engage CNS GIPR to achieve weight loss, especially given that a large molecule (>150 kD) would not be expected to cross the blood–brain barrier. Our findings show that both CNS *Gipr* and *Glp1r* expression are essential for the full body weight loss effects of mGIPR-Ab/GLP-1 peptide–antibody conjugates in mice. Notably, although the extent of weight loss is reduced in both CNS GLP-1R KO and CNS GIPR KO mice treated with mGIPR-Ab/GLP-1, it is not completely abolished, suggesting that each receptor contributes to the weight loss observed in control mGIPR-Ab/GLP-1-treated mice. Overall, these findings indicate that targeting both GIPR and GLP-1R in the CNS with peptide–antibody conjugates, enabling GIPR blockade together with GLP-1R agonism, enhances weight loss.

In addition to delivering meaningful weight loss, mGIPR-Ab/GLP-1 also provides metabolic benefits in downstream peripheral tissues. mGIPR-Ab/GLP-1 treatment of wild-type mice and KO of *Gipr* in the mouse CNS are both associated with similar downstream changes in gene expression related to cell cycle regulation, cholesterol biosynthesis, ECM and collagen organization, and immune response and inflammation in WAT and liver. These results, using either pharmacology or mouse genetics, show that reduction in CNS GIPR signalling can positively impact peripheral tissue metabolism. Indicators such as reduced cell cycle activity, ECM regulation and cholesterol biosynthesis may reflect reduced adipocyte growth and expansion^{43–45}. Specifically, genes related to lipid storage (CD36 molecule (*Cd36*), sterol regulatory element binding protein (*Srebp*)) and adipocyte differentiation (peroxisome proliferator activated receptor gamma (*Pparg*)) are significantly downregulated with reduced CNS GIPR signalling⁴⁶. Moreover, CNS GIPR KO and mGIPR-Ab/GLP-1 treatment of wild-type mice both result in reduced activity in pathways associated with immune function, particularly neutrophil degranulation, suggesting that decreased CNS GIPR signalling might reduce obesity-associated inflammation^{47–49}. These findings align with our plasma biomarker analyses demonstrating reduced plasma levels of the cytokines tumour necrosis factor

and MCP-1 in CNS GIPR KO mice, as well as existing literature showing that GLP-1R agonists targeted to CNS GLP-1R have anti-inflammatory effects²⁰. However, further investigation is needed to understand how these DEGs and pathways translate into the broader systemic effects that become evident following the engagement of CNS GIPR and GLP-1R.

Lastly, we provide evidence that the mGIPR-Ab/GLP-1 peptide–antibody conjugate accesses the CNS via the CVOs and activates neural pathways involved in regulating food intake and metabolism to induce weight loss. These data provide an explanation for CNS activation even though monoclonal antibodies have minimal brain penetrance, reaching concentrations of around 0.1–0.4% of the monoclonal antibody concentrations in the plasma^{50,51}. CVOs are highly permeable with fenestrated capillaries, allowing polypeptides to exit the brain and enabling substances like metabolic hormones and drugs, which typically do not cross the blood–brain barrier, to influence brain function^{52,53}. These findings provide a logical means by which peptide–antibody conjugates can trigger changes in brain activity. Peripherally administered GLP-1R and GIPR agonists have also been shown to localize in CVOs, with limited labelling in brain regions shielded by the blood–brain barrier^{13,54,55}. We also demonstrate here that mGIPR-Ab/GLP-1 peptide–antibody conjugates activate c-Fos in downstream brain regions, such as the nucleus of the solitary tract, parabrachial nucleus and central amygdalar nucleus. These c-Fos data shed light on neural substrates or neural pathways activated by mGIPR-Ab/GLP-1. We also demonstrate that each component of a mGIPR-Ab/GLP-1 peptide–antibody conjugate may act on different cell types and have differential effects on c-Fos within the AP. These data suggest that GIPR and GLP-1R are expressed on different cell populations in the AP, where GLP-1 also mediates nausea and avoidance⁵⁶. Future research will need to investigate specific cell types and the connectivity of these neural substrates to precisely map the neuroanatomical networks as well as the long-term (>4 h) activation of these neural substrates. Furthermore, targeted single-cell analysis focusing on gene expression changes in key brain regions is required to enhance our understanding of the molecular mechanism through which the mGIPR-Ab/GLP-1 peptide–antibody conjugate acts on key cell types and pathways to induce changes in eating behaviours and energy balance.

Overall, these findings are complementary to results in a companion article⁵⁷, in which the body-weight-reducing and food-intake-reducing effects of GIPR antagonism are disrupted in mice with global loss of either *Gipr* or *Glp1r* but preserved in mice with loss of *Gipr* in either GABAergic or peripheral neurons. Single-nucleus RNA-sequencing shows opposing effects of GIPR agonism and antagonism in the hindbrain, with antagonism, but not agonism, mimicking GLP-1R signalling and with GIPR antagonism and GLP-1R agonism both regulating gene programmes implicated in synaptic plasticity. Collectively, these findings support a model whereby the weight loss effects observed with GIPR antagonism require functional GLP-1R signalling. These data suggest that a mGIPR-Ab/GLP-1 peptide–antibody conjugate may act on a different population of cells or via distinct molecular mechanism(s) compared to GIPR agonists like tirzepatide. Future studies are needed to explore the interneural communication networks in key regions of the brain and signal transduction pathways through which GIPR antagonism recruits GLP-1R signalling.

In summary, we show that an mGIPR-Ab/GLP-1 peptide–antibody conjugate acts on both CNS GIPR and CNS GLP-1R, leading to additive effects on body weight loss in obese mice. The peptide–antibody conjugate accesses the CNS via CVOs, activating downstream brain regions involved in appetite regulation. These findings suggest that targeting accessible receptors in the CVOs of the brain could be a promising therapeutic strategy for the treatment of obesity. Future research should focus on identifying the specific cell types and molecular mechanisms targeted by mGIPR-Ab/GLP-1 peptide–antibody conjugates.

Our studies have some limitations, including the use of two distinct promoters to drive *cre* expression for targeting *Gipr* versus *Glp1r*

in the brain, and the non-CNS exclusive pattern of *Wnt1* expression, which also targets the enteric nervous system. Furthermore, CNS GIPR KO mice have a lower body weight than control mice; thus, there is a smaller window for weight loss, as body weight defence mechanisms have a greater role in lean mice, potentially confounding the absence of treatment effects. Interestingly, previous work⁵⁸ found that whole-body GIPR KO mice are not protected from DIO when housed at thermoneutrality. Therefore, conducting studies under thermoneutral conditions may provide a way to evaluate treatment effects in CNS GIPR KO mice independently of body weight defence mechanisms and temperature-associated thermogenesis. Moreover, body length and potential regulation of body growth may be different in CNS GIPR KO mice^{19,59}. Lastly, although female mice are generally more resistant to DIO and glucose intolerance, we observed no sex differences in the percentage of body weight loss in CNS GLP-1R KO mice treated with mGIPR-Ab/P1. However, a key limitation of our study is the predominant use of male mice. Future studies are needed to assess potential sex differences in the metabolic response to mGIPR-Ab/GLP-1 treatment in female mice.

Methods

All mice were housed at an AAALAC International-accredited facility. Animals were cared for in accordance with the *Guide for the Care and Use of Laboratory Animals*, 8th edition. All research protocols were reviewed and approved by the Amgen Institutional Animal Care and Use Committee (Thousand Oaks, CA), Toronto Centre for Phenogenomics at Mount Sinai Hospital (Toronto, Canada) and Danish Animal Experimentation Council (Hørsholm, Denmark). Lighting in animal holding rooms was maintained on a 12:12 h light-to-dark cycle, and the ambient temperature and humidity range was 20–26 °C and 30–70%, respectively. Animals had ad libitum access to irradiated pelleted feed and reverse-osmosis chlorinated (0.3–0.5 ppm) water via an automatic watering system. Body weight and food intake were measured as specified for each experiment. However, select food intake data points were excluded from analysis because of food shredding behaviour (noted at the time of measurement), so we were unable to obtain accurate measurements in food intake for all mice. Cages were changed weekly.

Data collection at the time of dosing was not performed blind to the conditions of the experiments, but all ex vivo analyses were blinded to the experimenter. Furthermore, no statistical methods were used to pre-determine sample sizes, but our sample sizes are similar to those reported in previous publications^{15–17}.

ICV administration of GIPR antibody

Male C57BL/6J mice from Jackson Laboratories or Envigo were fed a 60 kcal% fat diet (Research Diets, no. D12492i) for 20 weeks before ICV cannulation surgery and were 6 months old at the start of the study. For surgical implantation of the ICV cannula, mice were anaesthetised with 3–4% isoflurane (inhalation) during surgery and were given analgesic (carprofen, 5 mg kg^{−1}) and supplemental fluids (lactated Ringer's solution; 4 ml kg^{−1}) on surgery day and 1 day post-op. Daily body weight, food intake and health checks were conducted daily for 1 week and every 2–3 days thereafter. All mice recovered for 2 weeks post surgery before the start of dosing, and mice that did not recover within 3% of their pre-surgery body weight were removed from the study. During stereotaxic surgery (Kopf Instruments), mice received indwelling guide cannula (26-gauge, cut 2.75 mm below pedestal; P1 Technologies) targeting the third ventricle using the following stereotaxic coordinates, which are relative to the location of bregma at the skull surface: −0.88 mm anterior–posterior, +0.25 mm medial–lateral and −2.75 mm dorsal–ventral. Cannula were affixed to the skull using jeweler's screws (P1 Technologies) and acrylic resin (Lang Dental).

For central pharmacological delivery of drugs, mice were anaesthetised with 2.5–4% isoflurane. A 1 µl bolus injection was delivered at a rate of 1 µl min^{−1} using an infusion pump (Harvard Apparatus).

Dose response. Mice were randomized based on body weight and surgery date and assigned into one of six treatment groups: (1) artificial cerebrospinal fluid; (2) 15 μg IgG1; (3) 30 μg IgG1; (4) 7.5 μg GIPR-Ab; (5) 15 μg GIPR-Ab; or (6) 30 μg GIPR-Ab. Mice underwent ICV dosing every other day for ten treatments, and body weight and food intake were measured every day. At the end of the study, mice received 1 μl ICV injection of 1% Chicago Sky Blue, brain weight was recorded and cannula placement in the third ventricle was verified.

Central versus systemic comparison. All mice were ICV-cannulated. Mice were randomized based on body weight and day of ICV surgery, then assigned to one of four groups: (1) central GIPR-Ab, 15 μg ; (2) central IgG1, 15 μg ; (3) systemic GIPR-Ab, 5 mg kg^{-1} ; or (4) systemic IgG1 (5 mg kg^{-1}). Doses for comparing central and systemic administration of the GIPR-Ab were based on the highest efficacious dose in the previous experiment (Fig. 6a). Mice were dosed every other day for a total of seven treatments, and body weight and food intake were measured daily. At the end of the study, mice underwent a final post-study retro-orbital bleed, and brains, separated into forebrain and hindbrain (around -3.87 mm from bregma) and inguinal and epididymal WATs, were frozen in liquid nitrogen. Additionally, blood was collected from cardiac puncture for pharmacokinetic analysis 24 h after the last injection.

GIPR monoclonal antibody exposure. Quantitation of anti-GIPR monoclonal antibody in mouse plasma and tissues was performed using an electrochemiluminescent-based immunoassay. The method used biotinylated human GIPR protein (Amgen, lot no. 19457-1) as the capture reagent and ruthenylated mouse anti-human Fc (Amgen, lot no. 43509-4) as the detection reagent. Before drug quantitation, tissues were homogenized at 200 mg ml^{-1} in a Precellys Evolution homogenizer (Bertin Technologies) in a lysis buffer consisting of 50 mM Tris-HCl, 100 mM NaCl, 0.1% Triton X-100 pH 7.4 with 1 protease inhibitor (Roche A32955) for every 10 ml of buffer at 6,800 rpm for three 20 s cycles with 30 s pauses between cycles. The concentrations were interpolated from standard curves prepared in pooled mouse plasma using Watson LIMS software (ThermoFisher).

Generation of *Gipr*^{Syn^{-/-}} mice and *Glp1r*^{Wnt1^{-/-}} mice

Mice expressing Cre recombinase driven by the synapsin promoter were purchased from Jackson Laboratories (JAX, stock no. 003966)⁶⁰. Synapsin-Cre⁺ male mice were mated to *Gipr*^{fl/fl} female mice (previously described¹⁷) to generate mice with heterozygous floxed *Gipr* gene with or without the synapsin-Cre transgene. Heterozygous floxed *Gipr* female mice with the synapsin-Cre transgene were mated to heterozygous floxed *Gipr* male mice without the synapsin-Cre transgene to produce homozygous floxed *Gipr* (*Gipr*^{fl/fl}) mice with or without the synapsin-Cre transgene. Subsequent progenies were generated by mating *Gipr*^{fl/fl} male mice (no synapsin-Cre) with female homozygous floxed *Gipr* mice with the synapsin-Cre transgene (*Gipr*^{Syn^{-/-}}) to produce mice with CNSKO of *Gipr* (*Gipr*^{Syn^{-/-}}); their wild-type *Gipr*^{fl/fl} littermates were used as controls for all experiments.

Glp1r^{fl/fl} mice⁶¹ (generated and provided by R. Seeley, University of Michigan) and Wnt1-Cre2 mice were bred at Mount Sinai Hospital (Toronto, Canada), as previously described^{19,20}, to produce a CNS knock-down of the *Glp1r* (*Glp1r*^{Wnt1^{-/-}}). *Glp1r*^{Wnt1^{-/-}} mice and their Cre-negative floxed control (*Glp1r*^{fl/fl}) littermates were used for the study.

DIO *Gipr*^{Syn^{-/-}} and *Glp1r*^{Wnt1^{-/-}} mouse studies

Age-matched male *Gipr*^{fl/fl} and *Gipr*^{Syn^{-/-}} littermates were bred at Charles River Laboratories and shipped to Amgen at 7–9 weeks old, and age-matched *Glp1r*^{fl/fl} and *Glp1r*^{Wnt1^{-/-}} littermates were bred at Mount Sinai Hospital. Mice were singly housed and started HFD feeding (60 kcal% fat; Research Diets, D12492i) at an average of 9 weeks old for 12–14 weeks as indicated. Mice were randomized based on body

weight, then treated with either vehicle or mGIPR-Ab/P1 peptide–antibody conjugate every 6 days for 18 days. Food intake and body weight were measured every 2 days throughout the experimental period. Body composition was assessed by EchoMRI at baseline and on day 17 post treatment. On day 18, mice were killed, and brain, liver and WAT were collected and snap-frozen in liquid nitrogen. Plasma insulin was measured using a High Range Insulin ELISA kit for mouse (Alpco, cat. no. 80-INSMSH-E01), plasma lipids were measured through IDEXX bioanalytics and plasma hormones and immune metabolites were measured using the MAP Mouse Metabolic Hormone Expanded Panel (Milliplex, Cat. no. MMHE-44K).

Molecules used in chronic weight loss studies were generated by Amgen as previously described and dosing regimens for each molecule were established by previously published pharmacokinetic and pharmacodynamic studies: mGIPR-Ab (25 mg kg^{-1} every 6 days)¹⁷, dulaglutide (0.3 mg kg^{-1} every 3 days)¹⁷ and mGIPR-Ab/P1 or mGIPR-Ab/P3 (1.5 mg kg^{-1} every 6 days)¹⁶. All IP injections were performed at 2 ml kg^{-1} , and molecules were formulated in vehicle buffer (10 mM acetate and 9% sucrose, pH 5.2).

During the study, body weight and food intake were measured every 2–3 days as indicated and body composition was measured pre-treatment and post-treatment as indicated by nuclear magnetic resonance (EchoMRI). Mice were fasted for 4 h in the morning and killed by conscious decapitation. Blood glucose was measured by glucometer (AlphaTrak), and blood was processed to plasma and stored frozen at -80°C . Tissues were dissected, weighed and flash-frozen in liquid nitrogen. Plasma insulin was measured using the High Range Mouse Insulin ELISA (Alpco), and plasma total cholesterol was measured using the Wako Cholesterol E colorimetric assay (Fujifilm) following the manufacturer's instructions.

Whole brains were collected and immediately frozen in liquid nitrogen. Brains were later sectioned on Leica CM3000 cryostat, and 1 mm punches (Integra Miltex Biopsy Punch) of the hypothalamus, hippocampus and hindbrain were collected. Pancreatic islets were isolated as previously described¹⁷ from mice killed by terminal decapitation and the peritoneal cavity exposed. The sphincter of Oddi was clamped, and 4–6 ml of cold enzyme buffer (1 \times Hanks' Balanced Salt Solution, 25 mM HEPES, 100 mg l^{-1} DNase I, 1 \times penicillin–streptomycin with glutamine)/collagenase (1 mg ml^{-1}) was introduced through the bile duct. Following inflation, the pancreas was removed and transferred to a 50 ml falcon tube containing 5 ml enzyme buffer/collagenase on ice. The pancreas was digested at 37°C for 10–20 min, and the tube was then shaken by hand five to ten times. The digestion was stopped by adding 50 ml cold quenching buffer (enzyme buffer + 10% FBS). The islets were collected by centrifugation at 300g for 2 min. The supernatant was removed, and the islet pellet was resuspended in 50 ml quenching buffer and spun again at 300g. Following the two washes, the islet pellet was put on a three-level histopaque (Sigma) gradient and spun 30 min at 1,000g, with the centrifuge brake turned off. Following centrifugation, the purified islets were removed from the middle layer and placed into a fresh culture dish containing RPMI. From there, the islets were placed into 2 ml Eppendorf tubes and frozen at -80°C in TRIzol (Invitrogen) for RNA analysis.

RNA was isolated from brain and islets using RNeasy micro kit (Qiagen), cDNA was synthesized from equal amounts of RNA using SuperScript III First-Strand Synthesis kit (Invitrogen) and gene expression was quantified using PowerUp Sybr Green Reagents (Invitrogen) according to the manufacturers' instructions. The following primer pairs were used for *Gipr* expression normalized to Eukaryotic elongation factor 2 (*Eef2*): *Gipr* F, TTGTGTGGGAGCCAATTACA; *Gipr* R, ACC-CAGGGAATGACGAAAAG; *Eef2* F, AGCGAGGACAAAGACAAGGA; *Eef2* R, GGGATGGTAAGTGGATGGTG.

In vitro cAMP assay

For GLP-1R agonist activity, CHOK1 cells stably expressing human GLP-1R were used to measure peptide–antibody conjugate-induced

cAMP production in a homogenous time-resolved fluorescence assay (Cisbio, cat. no. 62AM4PEJ). Serially diluted peptide–antibody conjugates were incubated with 40,000 cells in assay buffer (0.1% BSA, 500 μ M 3-isobutyl-1-methylxanthine in F12 media) for 15 min at 37 °C. Cells were then lysed with lysis buffer containing cAMP-d2 and cAMP cryptate (Cisbio) and incubated for 1 h at 20–22 °C before measurement in the EnVision plate reader (PerkinElmer). The cAMP levels are expressed as a fluorescence ratio of 665/620 nm.

For GIPR antagonist activity, HEK293T cells stably expressing human GIPR were used to measure peptide or peptide–antibody conjugate-induced cAMP production in a homogenous time-resolved fluorescence assay (Cisbio, cat. no. 62AM4PEJ). Serially diluted GIPR-Ab was incubated with 30,000 cells in assay buffer (0.1% BSA, 500 mM 3-isobutyl-1-methylxanthine in F12 media) for 30 min at 37 °C before treatment with GIP at a final concentration of 0.05 nM. Cells were incubated for 30 min at 37 °C and then lysed in lysis buffer containing cAMP-d2 and cAMP cryptate (Cisbio) for 1 h at room temperature. The fluorescence was measured in an EnVision plate reader (PerkinElmer), and cAMP levels are expressed as a ratio of 665/620 nm.

Bulk RNA-sequencing of liver and WAT

RNA extraction, library construction and sequencing. To assess changes in gene expression in peripheral tissues, liver and inguinal WAT collected from DIO *Gipr^{Syn-/-}* and *Glp1r^{Wnt1-/-}* mice with mGIPR-Ab/P1 peptide–antibody conjugate treatment (Figs. 4 and 5) were processed and analysed using bulk RNA-sequencing. It is important to note that these data were obtained using a surrogate molecule and may not be directly extrapolated to the clinical candidate, Maridebart Cafraglutide (MariTide). For the extraction of total RNA, tissue samples were pulverized using GenoGrinder (Cole–Parmer), then homogenized in Tri Reagent (Molecular Research Center or Ambion by Life Technologies) using a MagNa Lyser or TissueLyser II system (Qiagen). mRNA was then chloroform-extracted and precipitated using isopropanol and washed with 75% ethanol or precipitated using the RNeasy Plus 96 Kit (Qiagen). RNA was reconstituted with DEPC-treated water.

Sequencing libraries were constructed from RNA samples using the TruSeq Stranded mRNA Library Prep Kit (Illumina) and IDT for Illumina-TruSeq RNA UD Indexes. Libraries were pooled and sequenced on a NovaSeq X sequencing system (Illumina). Following sample demultiplexing, sequencing reads were aligned to the mouse B39 reference genome using the Omicsoft OSA alignment software (Qiagen). The gene annotation model was a hybrid model adopted from the Omicsoft (Qiagen) and GenCode (v28) gene models. Aligned reads were quantified at the gene level using an expectation maximization method (RSEM) and gene counts were combined across samples into a sample-by-gene count matrix.

DEGs and pathway analysis. The raw gene counts were normalized and processed for differential expression gene analysis using DESeq2 (v.1.38.3)⁵⁹. Specifically, genes with low expression (average fragments per kilobase of transcript per million mapped reads in each group of <1) were removed from the analysis. Gene counts were normalized to size factor for each sample. To examine the pharmacological effects of mGIPR-Ab/P1 treatment, *Gipr^{fl/fl}*, mGIPR-Ab/P1 versus *Gipr^{fl/fl}* vehicle and *Glp1r^{fl/fl}* mGIPR-Ab/P1 versus *Glp1r^{fl/fl}* vehicle were compared. To examine the contribution of CNS receptor expression, *Gipr^{Syn-/-}* vehicle versus *Gipr^{fl/fl}* vehicle and *Glp1r^{Wnt1-/-}* vehicle versus *Glp1r^{fl/fl}* vehicle were compared. The significantly expressed genes were determined by a false discovery rate of <0.05 and fold change of >1.5 from the Wald Test. Ingenuity Pathway Analysis (Qiagen, v.111725566) was applied to canonical pathway analysis. Normalized gene count (variance stabilizing transformation in DESeq2) was used for heatmap visualization. The colour was scaled across samples for each gene. Heatmap and bubble plots were generated using the R packages ggplot2 (v.3.4.30) and pheatmap (v.1.0.12).

c-FOS and human IgG immunostaining

Biodistribution and whole-brain c-Fos analysis. The control antibody (IgG1) and c-Fos immunostaining study was conducted at Gubra (Hørsholm, Denmark). Singly housed male C57BL/6J mice were fed a 60 kcal% fat diet (Research Diets, D12492) for 16 weeks. Mice were 24 weeks old at the start of the study and were randomized based on body weight into study groups ($n = 8$ per group) and mock-handled from day –4 to day 1. Body weight was measured throughout the study. On day 1, each mouse was administered an IP dose of either vehicle or GIPR-Ab/GLP-1 at a dosage of 10 nmol kg⁻¹. Mice were fasted for 4 h before being killed (4 h post dosing), and brains were perfused with 10% neutral buffered formalin under isoflurane anaesthesia.

Brains were isolated and stained for human immunoglobulin G (hIgG) and c-Fos. Samples were fixed overnight in 10% neutral buffered formalin and washed on the following day for 1 h in PBS. Samples were then dehydrated in a methanol and H₂O gradient: 20%, 40%, 60%, 80% and 100% methanol, each step for 1 h at room temperature. They were further washed in 100% methanol for 1 h and incubated overnight in 66% dichloromethane (DCM) and 33% methanol at room temperature. The next day, the samples were washed twice in 100% methanol for 30 min, cooled down to 4 °C in 1 h and bleached in chilled fresh 5% H₂O₂ in methanol (one volume 35% H₂O₂ to six times volume methanol) overnight at 4 °C. The samples were subsequently rehydrated in a methanol and PBS series: 80%, 60%, 40% and 20%, with 0.2% Triton X-100, 1 h each at room temperature. They were washed in PBS with PTx.2 (0.2% Triton X-100) for 2 × 1 h at room temperature. Samples were incubated in permeabilization solution at 37 °C for 3 days. Blocking was carried out in blocking solution (42 ml PTx.2, 3 ml donkey serum, 5 ml dimethylsulfoxide, 0.02% sodium azide) at 37 °C for 2 days. The samples were incubated with primary antibody (rabbit anti-c-Fos; Cell Signaling, ab2250S, 1:5,000) in PTwH (100 PBS 10×, 2 ml Tween 20, 1 ml of 10 mg ml⁻¹ heparin stock solution) and 5% dimethylsulfoxide and 3% donkey serum at 37 °C for 7 days. Next, they were washed in PTwH (100 PBS 10×, 2 ml Tween 20, 1 ml of 10 mg ml⁻¹ heparin stock solution) for 1 × 10 min, 1 × 20 min, 1 × 30 min, 1 × 1 h, 1 × 2 h and 1 × 2 days. Samples were incubated with secondary antibody (donkey anti-rabbit Cy5; Jackson ImmunoResearch, 1:1,000 and donkey anti-human AF790; Jackson ImmunoResearch, 1:400) in PTwH (100 PBS 10×, 2 ml Tween 20, 1 ml of 10 mg ml⁻¹ heparin stock solution) and 3% donkey serum at 37 °C for 7 days, followed by washes in PTwH (100 PBS 10×, 2 ml Tween 20, 1 ml of 10 mg ml⁻¹ heparin stock solution): 1 × 10 min, 1 × 20 min, 1 × 30 min, 1 × 1 h, 1 × 2 h and 1 × 3 days. All steps were performed in tightly closed tubes to minimize evaporation and oxidation.

Brains were cleared using iDISCO standard protocol^{62,63}. In brief, tissue was cleared in a methanol and H₂O series: 20%, 40%, 60%, 80% and 100% for 1 h each at room temperature. Samples were incubated in 100% methanol overnight and the next day for 3 h (with shaking) in 66% DCM and 33% methanol at room temperature and in 100% DCM 15 min twice (with shaking) to remove traces of methanol. The samples were finally transferred to ethyl cinnamate and stored in closed vials. Samples were then imaged using a light-sheet microscope (LCS SPIM microscope with ×4 C objective). Whole-brain quantification of c-Fos⁺ cells and the compound fluorescence was performed, mapped to an atlas and compared across groups (Imaris v.2; Oxford Instruments).

***Gipr* and *Glp1r* in situ hybridization in the AP.** Formalin-fixed, paraffin-embedded brains were collected from DIO (60 kcal% fat; Research Diets, no. D12492i) wild-type male adult mice (~20 weeks old). Fully automated mRNA in situ hybridization (ISH) was performed using the Leica Biosystems BOND RX platform and the ready-to-use RNAscope 2.5 LSx reagent kit-red (single ISH kit, cat. no. 322750) and RNAscope 2.5 LSx duplex assay (duplex ISH kit, cat. no. 322440) combined with Leica reagents. Mm-*Gipr* (cat. no. 319128-C2), Mm-*Glp1r* (cat. no. 418858), Mm-Polr2a-C2/Mm-PPIB-C1 (cat. no. 320768), dapB-C1/DapB-C2 (cat. no. 320758) and PPIB (cat. no. 313918) probes

were purchased from Advanced Cell Diagnostics. Hybridization was detected with Leica bond polymer refined red detection kit (cat. no. DS939) and Leica bond polymer refined DAB detection kit (cat. no. DS9800) and Leica green chromogen (cat. no. DC991), then counterstained with hematoxylin. Slides were washed with double-distilled water once (one dip), then 0.02% ammonia hydroxide (five dips) and then dried in a 60 °C oven for 2 h and coverslipped using VectaMount Permanent Mounting Medium (Advanced Cell Diagnostics, cat. no. 321584). Light microscopic analysis of tissues was conducted using an Aperio GT 450 scanner at $\times 40$ (Leica Biosystems, cat. no. 23GT450). The quality of each tissue was evaluated using H&E-stained sections and PPIB and Polr2a/PPIB ISH stains. Samples with PPIB ISH scores of ≥ 2 (noted as positive) and dapB ISH scores of 0 (noted as negative) were considered to have adequate tissue viability, and GIPR and GLP-1R mRNA ISH were evaluated. Tissues that did not meet qualitative standards of adequate PPIB were excluded from further analysis.

GIPR and GLP-1R mRNA ISH images were evaluated, and scores were provided in accordance with the following modified ACD scoring criteria: 0, no staining or <1 dot per ten cells; 1, one to three dots per cell; 2, four to nine dots per cell, no or very few dot clusters; 3, 10–15 dots per cell and/or $<10\%$ dots in cluster; 4, >15 dots per cell and/or $>10\%$ dots in cluster. The scoring was reviewed by a board-certified veterinary pathologist.

c-Fos fluorescent immunohistochemistry in the AP. To examine mGIPR-Ab and GIPR-Ab/GLP-1 possible antagonistic effect on DA-GIP-induced c-FOS, DIO (60 kcal% fat; Research Diets, no. D12492i) male C57BL/6 mice (6 months old) were randomized based on body weight and received pre-treatment of IgG1, GIPR-Ab (5 mg kg⁻¹) or GIPR-Ab/GLP-1 (1.5 mg kg⁻¹), dosed 24 h before an assay treatment of vehicle or [D-Ala²]-GIP (100 nmol kg⁻¹, human; Phoenix Pharmaceuticals). Then, 4 h later, mice were anaesthetised with 4–5% isoflurane, and brains were perfused with 0.9% saline followed by 10% formalin. Brains were ‘sunk’ in 12% sucrose in formalin (10%) overnight and frozen using dry ice-chilled 2-methylbutane. Brains were sliced on a sliding microtome (Leica), and serial 30 μ m coronal sections were collected in antifreeze and stored at –20 °C until further processing. For c-FOS immunohistochemistry, sections containing AP were washed 6 \times 5 min with KPBS. The tissue was permeabilized with 0.3% Triton X solution for 30 min, followed by 3 \times 5 min washes with KPBS. Tissue was then blocked with 2% normal donkey serum for 30 min and incubated with rabbit anti-c-FOS primary antibody (1:1,500; Synaptic Systems) overnight at 4 °C. Sections were washed 6 \times 10 min with KPBS and placed in goat anti-rabbit AF Plus 488 secondary antibody (1:500, Invitrogen) for 2 h at room temperature. Sections were mounted on slides and imaged using a Leica SP8 confocal microscope and Leica LAS X software. c-Fos⁺ cells were quantified using ImageJ software (version 1.54j).

Statistical analysis

One-way or two-way ANOVA followed by Tukey’s or Šidák’s test for multiple comparisons (with repeated measures for time-series data) was used, as noted in figure legends. For comparison between two groups, Student’s *t*-test was performed. Statistics were calculated using GraphPad Prism 8 (v.8.4.3 (686)). Data distribution for in vivo pharmacology studies was assumed to be normal, but this was not formally tested. Refer to source data for post-hoc *t*-test results.

The c-Fos analyses for each region were conducted with a negative binomial generalized linear model, and a subsequent Dunnett’s test was performed for multiple comparisons. All significantly regulated regions among the preselected 12 regions as well as the 800+ regions went through statistical validation, in which the model deviance residuals were investigated to determine whether they aligned with the assumptions of normality and homoscedasticity. Cook’s distance was evaluated for each data point to ensure no point was overly influential in the fitted model.

RNA-sequencing data were analysed using right-tailed Fisher’s exact test within the Ingenuity Pathway Analysis database.

Data and materials availability

All source data associated with each figure is provided. The liver and WAT gene expression data have been deposited in Gene Expression Omnibus under accession code GSE293291. Reagents can be provided by and at Amgen’s sole discretion, pending scientific review and a completed material transfer agreement with Amgen. Requests from an academic or nonprofit institution should be submitted at wwwext.amgen.com/partners/academic-collaborations/new-requests. Requests from a for-profit entity should be submitted to BDopportunities@amgen.com.

Reporting summary

Further information on research design is available in the Nature Portfolio Reporting Summary linked to this article.

Code availability

No code was developed in this study.

References

1. Liu, C. M. & Kanoski, S. E. Homeostatic and non-homeostatic controls of feeding behavior: distinct vs. common neural systems. *Physiol. Behav.* **193**, 223–231 (2018).
2. Watts, A. G., Kanoski, S. E., Sanchez-Watts, G. & Langhans, W. The physiological control of eating: signals, neurons, and networks. *Physiol. Rev.* **102**, 689–813 (2022).
3. Cheng, W. et al. Hindbrain circuits in the control of eating behaviour and energy balance. *Nat. Metab.* **4**, 826–835 (2022).
4. Chen, Y., Lin, Y. C., Kuo, T. W. & Knight, Z. A. Sensory detection of food rapidly modulates arcuate feeding circuits. *Cell* **160**, 829–841 (2015).
5. Meye, F. J. & Adan, R. A. Feelings about food: the ventral tegmental area in food reward and emotional eating. *Trends Pharmacol. Sci.* **35**, 31–40 (2014).
6. Hernandez, L. & Hoebel, B. G. Food reward and cocaine increase extracellular dopamine in the nucleus accumbens as measured by microdialysis. *Life Sci.* **42**, 1705–1712 (1988).
7. Salamone, J. D., Correa, M., Mingote, S. & Weber, S. M. Nucleus accumbens dopamine and the regulation of effort in food-seeking behavior: implications for studies of natural motivation, psychiatry, and drug abuse. *J. Pharmacol. Exp. Ther.* **305**, 1–8 (2003).
8. Müller, T. D. et al. Glucagon-like peptide 1 (GLP-1). *Mol. Metab.* **30**, 72–130 (2019).
9. Kaplan, A. M. & Vigna, S. R. Gastric inhibitory polypeptide (GIP) binding sites in rat brain. *Peptides* **15**, 297–302 (1994).
10. Dowsett, G. K. C. et al. A survey of the mouse hindbrain in the fed and fasted states using single-nucleus RNA sequencing. *Mol. Metab.* **53**, 101240 (2021).
11. Adriaenssens, A. E. et al. Glucose-dependent insulinotropic polypeptide receptor-expressing cells in the hypothalamus regulate food intake. *Cell Metab.* **30**, 987–996.e6 (2019).
12. Steuernagel, L. et al. HypoMap—a unified single-cell gene expression atlas of the murine hypothalamus. *Nat. Metab.* **4**, 1402–1419 (2022).
13. Adriaenssens, A. et al. Hypothalamic and brainstem glucose-dependent insulinotropic polypeptide receptor neurons employ distinct mechanisms to affect feeding. *JCI Insight* **8**, e164921 (2023).
14. Jastreboff, A. M. et al. Tirzepatide once weekly for the treatment of obesity. *N. Engl. J. Med.* **387**, 205–216 (2022).
15. Véniant, M. M. et al. A GIPR antagonist conjugated to GLP-1 analogues promotes weight loss with improved metabolic parameters in preclinical and phase 1 settings. *Nat. Metab.* **6**, 290–303 (2024).

16. Lu, S. C. et al. GIPR antagonist antibodies conjugated to GLP-1 peptide are bispecific molecules that decrease weight in obese mice and monkeys. *Cell Rep. Med.* **2**, 100263 (2021).
17. Killion, E. A. et al. Anti-obesity effects of GIPR antagonists alone and in combination with GLP-1R agonists in preclinical models. *Sci. Transl. Med.* **10**, eaat3392 (2018).
18. Zhang, Q. et al. The glucose-dependent insulinotropic polypeptide (GIP) regulates body weight and food intake via CNS-GIPR signaling. *Cell Metab.* **33**, 833–844.e5 (2021).
19. Varin, E. M. et al. Distinct neural sites of GLP-1R expression mediate physiological versus pharmacological control of incretin action. *Cell Rep.* **27**, 3371–3384.e3 (2019).
20. Wong, C. K. et al. Central glucagon-like peptide 1 receptor activation inhibits Toll-like receptor agonist-induced inflammation. *Cell Metab.* **36**, 130–143.e5 (2024).
21. Greiner, E. M. & Petrovich, G. D. Recruitment of hippocampal and thalamic pathways to the central amygdala in the control of feeding behavior under novelty. *Brain Struct. Funct.* **229**, 1179–1191 (2024).
22. Schnapp, W. I. et al. Development of activity-based anorexia requires PKC- δ neurons in two central extended amygdala nuclei. *Cell Rep.* **43**, 113933 (2024).
23. Naka, T. et al. Activation of β -adrenoceptors in the bed nucleus of the stria terminalis induces food intake reduction and anxiety-like behaviors. *Neuropharmacology* **67**, 326–330 (2013).
24. Qiao, H., Ren, W. N., Li, H. Z. & Hou, Y. X. Inhibitory effects of peripheral administration of exendin-4 on food intake are attenuated by lesions of the central nucleus of amygdala. *Brain Res. Bull.* **148**, 131–135 (2019).
25. Kim, J. H. et al. A discrete parabrachial nucleus subpopulation plays a critical role in appetite suppression. *Elife* **11**, e75470 (2022).
26. Ding, W., Weltzien, H., Peters, C. & Klein, R. Nausea-induced suppression of feeding is mediated by central amygdala Dlk1-expressing neurons. *Cell Rep.* **43**, 113990 (2024).
27. Sabatini, P. V. et al. GFRAL-expressing neurons suppress food intake via aversive pathways. *Proc. Natl Acad. Sci. USA* **118**, e2021357118 (2021).
28. Campos, C. A., Bowen, A. J., Schwartz, M. W. & Palmiter, R. D. Parabrachial CGRP neurons control meal termination. *Cell Metab.* **23**, 811–820 (2016).
29. Wu, Q., Clark, M. S. & Palmiter, R. D. Deciphering a neuronal circuit that mediates appetite. *Nature* **483**, 594–597 (2012).
30. Kanoski, S. E., Alhadeff, A. L., Fortin, S. M., Gilbert, J. R. & Grill, H. J. Leptin signaling in the medial nucleus tractus solitarius reduces food seeking and willingness to work for food. *Neuropsychopharmacology* **39**, 605–613 (2014).
31. Adriaenssens, A. E., Gribble, F. M. & Reimann, F. The glucose-dependent insulinotropic polypeptide signaling axis in the central nervous system. *Peptides* **125**, 170194 (2020).
32. Jensen, C. B. et al. Characterization of the glucagonlike peptide-1 receptor in male mouse brain using a novel antibody and in situ hybridization. *Endocrinology* **159**, 665–675 (2018).
33. Kaneko, K. et al. Gut-derived GIP activates central Rap1 to impair neural leptin sensitivity during overnutrition. *J. Clin. Invest.* **129**, 3786–3791 (2019).
34. NamKoong, C. et al. Central administration of GLP-1 and GIP decreases feeding in mice. *Biochem. Biophys. Res. Commun.* **490**, 247–252 (2017).
35. Ambati, S. et al. GIP-dependent expression of hypothalamic genes. *Physiol. Res.* **60**, 941–950 (2011).
36. Killion, E. A. et al. Glucose-dependent insulinotropic polypeptide receptor therapies for the treatment of obesity, do agonists = antagonists? *Endocr. Rev.* **41**, 1–21 (2020).
37. Killion, E. A. et al. Chronic glucose-dependent insulinotropic polypeptide receptor (GIPR) agonism desensitizes adipocyte GIPR activity mimicking functional GIPR antagonism. *Nat. Commun.* **11**, 4981 (2020).
38. Kizilkaya, H. S. et al. Characterization of genetic variants of GIPR reveals a contribution of β -arrestin to metabolic phenotypes. *Nat. Metab.* **6**, 1268–1281 (2024).
39. Liskiewicz, A. et al. Glucose-dependent insulinotropic polypeptide regulates body weight and food intake via GABAergic neurons in mice. *Nat. Metab.* **5**, 2075–2085 (2023).
40. Wean, J. et al. Specific loss of GIPR signaling in GABAergic neurons enhances GLP-1R agonist-induced body weight loss. *Mol. Metab.* **95**, 102074 (2025).
41. Miyawaki, K. et al. Inhibition of gastric inhibitory polypeptide signaling prevents obesity. *Nat. Med.* **8**, 738–742 (2002).
42. Bernal, A. & Arranz, L. Nestin-expressing progenitor cells: function, identity and therapeutic implications. *Cell. Mol. Life Sci.* **75**, 2177–2195 (2018).
43. Li, Q. & Spalding, K. L. The regulation of adipocyte growth in white adipose tissue. *Front. Cell Dev. Biol.* **10**, 1003219 (2022).
44. Ruiz-Ojeda, F. J. et al. Active integrins regulate white adipose tissue insulin sensitivity and brown fat thermogenesis. *Mol. Metab.* **45**, 101147 (2021).
45. Iwayama, T. et al. PDGFR α signaling drives adipose tissue fibrosis by targeting progenitor cell plasticity. *Genes Dev.* **29**, 1106–1119 (2015).
46. Soyak, S. M., Nofziger, C., Dossena, S., Paulmichl, M. & Patsch, W. Targeting SREBPs for treatment of the metabolic syndrome. *Trends Pharmacol. Sci.* **36**, 406–416 (2015).
47. Uribe-Querol, E. & Rosales, C. Neutrophils actively contribute to obesity-associated inflammation and pathological complications. *Cells* **11**, 1883 (2022).
48. Choi, Y. et al. Serpina3c regulates adipogenesis by modulating insulin growth factor 1 and integrin signaling. *iScience* **23**, 100961 (2020).
49. Sekimoto, R. et al. High circulating levels of S100A8/A9 complex (calprotectin) in male Japanese with abdominal adiposity and dysregulated expression of S100A8 and S100A9 in adipose tissues of obese mice. *Biochem. Biophys. Res. Commun.* **419**, 782–789 (2012).
50. Garg, A. & Balthasar, J. P. Investigation of the influence of FcRn on the distribution of IgG to the brain. *AAPS J.* **11**, 553–557 (2009).
51. Shah, D. K. & Betts, A. M. Antibody biodistribution coefficients: inferring tissue concentrations of monoclonal antibodies based on the plasma concentrations in several preclinical species and human. *MAbs* **5**, 297–305 (2013).
52. Ganong, W. F. Circumventricular organs: definition and role in the regulation of endocrine and autonomic function. *Clin. Exp. Pharm. Physiol.* **27**, 422–427 (2000).
53. Buller, S. & Blouet, C. Brain access of incretins and incretin receptor agonists to their central targets relevant for appetite suppression and weight loss. *Am. J. Physiol. Endocrinol. Metab.* **326**, E472–E480 (2024).
54. Gabery, S. et al. Semaglutide lowers body weight in rodents via distributed neural pathways. *JCI Insight* **5**, e133429 (2020).
55. Samms, R. J. et al. GIPR agonism inhibits PYY-induced nausea-like behavior. *Diabetes* **71**, 1410–1423 (2022).
56. Zhang, C. et al. Area postrema cell types that mediate nausea-associated behaviors. *Neuron* **109**, 461–472.e465 (2021).
57. Müller, T. D. et al. GIPR agonism and antagonism decrease body weight and food intake via different mechanisms in male mice. *Nat. Metab.* <https://doi.org/10.1038/s42255-025-01294-x> (2025).
58. Furber, E. C. et al. GIPR agonism enhances TZD-induced insulin sensitivity in obese IR mice. *Diabetes* **73**, 292–305 (2024).

59. Love, M. I., Huber, W. & Anders, S. Moderated estimation of fold change and dispersion for RNA-seq data with DESeq2. *Genome Biol.* **15**, 550 (2014).
60. Zhu, Y. et al. Ablation of NF1 function in neurons induces abnormal development of cerebral cortex and reactive gliosis in the brain. *Genes Dev.* **15**, 859–876 (2001).
61. Sisley, S. et al. Neuronal GLP1R mediates liraglutide's anorectic but not glucose-lowering effect. *J. Clin. Invest.* **124**, 2456–2463 (2014).
62. Hansen, H. H. et al. Whole-brain activation signatures of weight-lowering drugs. *Mol. Metab.* **47**, 101171 (2021).
63. Perens, J. et al. An optimized mouse brain atlas for automated mapping and quantification of neuronal activity using iDISCO+ and light sheet fluorescence microscopy. *Neuroinformatics* **19**, 433–446 (2021).

Acknowledgements

We acknowledge the Cardiometabolic Disorders team at Amgen Research for their valuable contributions to this work. We also acknowledge J. Falsey, B. Wu, Y. Cheng and K. Walker for generously providing test materials. B. Amer, A. Mogul, A. Syverud and K. Shant also provided their expertise and assistance with drug formulation for neuropharmacology experiments. Lastly, we thank E. Gillespie, who aided in medical writing support. Amgen Inc. funded this work. D.J.D. is supported by a Banting and Best Diabetes Centre Novo Nordisk Chair in Incretin biology and a Sinai Health Novo Nordisk Foundation Fund in Regulatory Peptides as well as Canadian Institute for Health Research (CIHR) grant 192044. R.H. is supported by a Canadian Institute for Health Research postdoctoral fellowship.

Author contributions

C.-M.L., E.A.K., R.H., S.-C.L., R.K., D.J.D. and M.M.V. conceived and designed the study. C.-M.L., E.A.K., R.H., S.-C.L., R.K., T.L., M.K., V.A.T., K.C., G.N.S., A.B.B., L.A., R.H., A.T., A.S., C.-M.L., D.J.D. and M.M.V. acquired data. C.-M.L., E.A.K., R.H., S.-C.L., R.K., D.J.D. and M.M.V. analysed and interpreted the data.

Competing interests

All authors, with the exception of D.J.D. and R.H., are or were employees or contractors of Amgen and have received Amgen stock. Most of the work has been included in patent no. PCT/US2016/068138: 'Method of treating or ameliorating metabolic disorders using binding proteins for gastric inhibitory peptide receptor (GIPR) in combination

with GLP-1 agonists.' D.J.D. has served as a consultant or speaker within the past 12 months to Amgen, AstraZeneca, Insulet, Kallyope, Novo Nordisk and Pfizer. D.J.D. holds non-exercised options in Kallyope.

Additional information

Extended data is available for this paper at <https://doi.org/10.1038/s42255-025-01295-w>.

Supplementary information The online version contains supplementary material available at <https://doi.org/10.1038/s42255-025-01295-w>.

Correspondence and requests for materials should be addressed to Murielle M. Véniant.

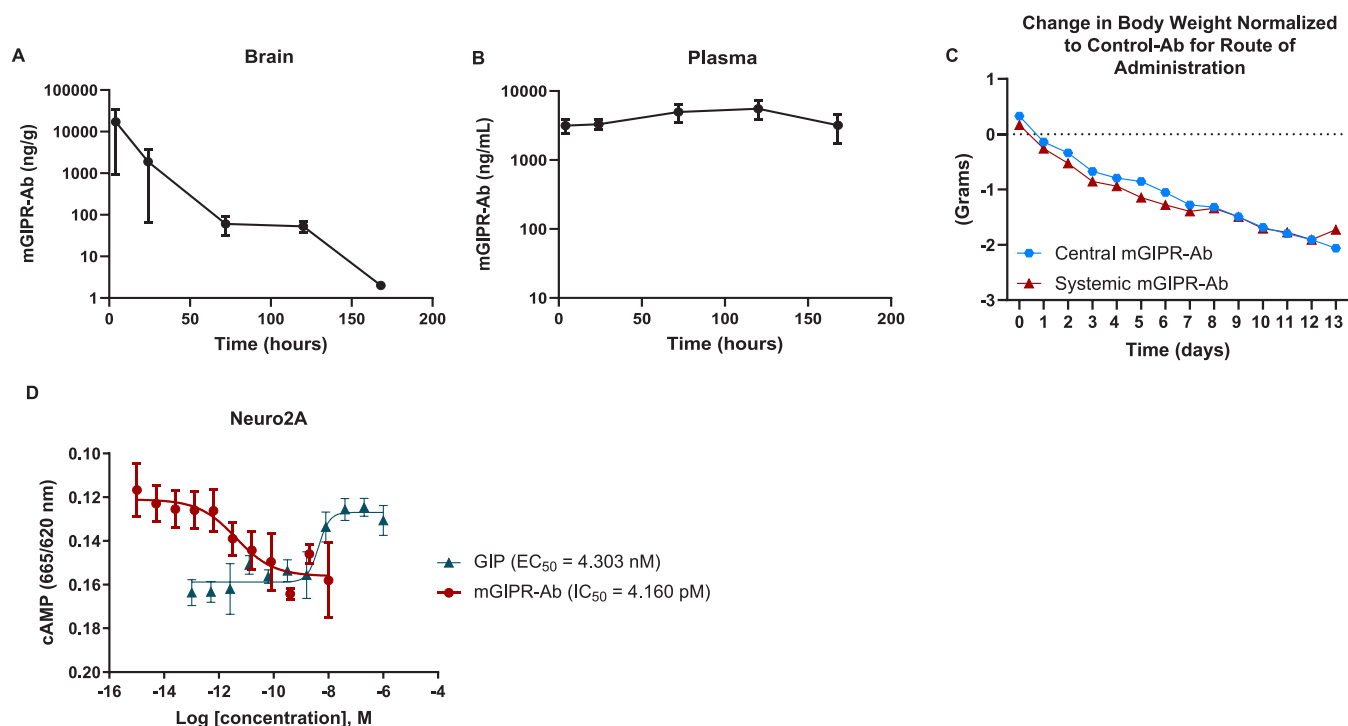
Peer review information *Nature Metabolism* thanks Alice Adriaenssens, Nigel Irwin and the other, anonymous, reviewer(s) for their contribution to the peer review of this work. Primary Handling Editor: Christoph Schmitt, in collaboration with the *Nature Metabolism* team.

Reprints and permissions information is available at www.nature.com/reprints.

Publisher's note Springer Nature remains neutral with regard to jurisdictional claims in published maps and institutional affiliations.

Open Access This article is licensed under a Creative Commons Attribution-NonCommercial-NoDerivatives 4.0 International License, which permits any non-commercial use, sharing, distribution and reproduction in any medium or format, as long as you give appropriate credit to the original author(s) and the source, provide a link to the Creative Commons licence, and indicate if you modified the licensed material. You do not have permission under this licence to share adapted material derived from this article or parts of it. The images or other third party material in this article are included in the article's Creative Commons licence, unless indicated otherwise in a credit line to the material. If material is not included in the article's Creative Commons licence and your intended use is not permitted by statutory regulation or exceeds the permitted use, you will need to obtain permission directly from the copyright holder. To view a copy of this licence, visit <http://creativecommons.org/licenses/by-nc-nd/4.0/>.

© The Author(s) 2025

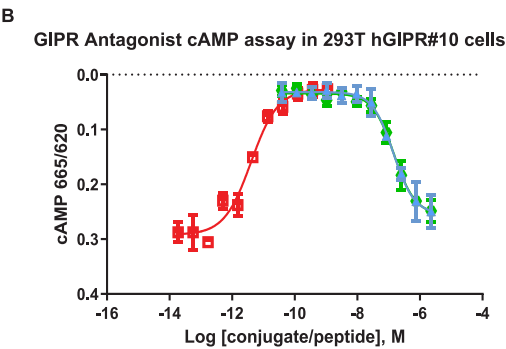


Extended Data Fig. 1 | In vivo pharmacokinetic profile and in vitro activity of mGIPR-Ab. To determine dose level and dose frequency of central administration of mGIPR-Ab, pharmacokinetic profile of (a) brain and (b) plasma exposure was assessed at 4, 24, 72, 120, and 168 h following a single ICV injection of 15 μ g/ μ L/mouse dose of mGIPR-Ab. To evaluate and compare weight loss from ICV vs. IP mGIPR-Ab treatment, (c) change in body weight was normalized to change in body weight in IgG1 control antibody treatment group with corresponding route of administration. To define meaningful levels of exposure in vivo, (d) mGIPR-Ab antagonist inhibition of GIP-induced cAMP production was measured in neuro2A cells (mGIPR-Ab run in technical quadruplicates and

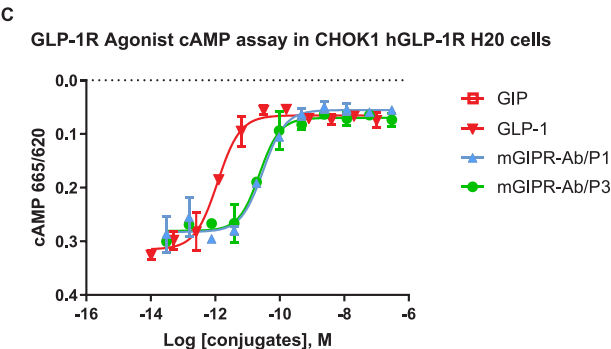
GIP run in technical duplicates). In vitro IC_{50} value of mGIPR-Ab could then be used to compare with exposure levels in brain, plasma, and peripheral tissues following central or systemic administration of mGIPR-Ab in diet-induced obese male mice. (A-B) 4 h (n=3), 24 h (n=3), 72 h (n=3), 120 h (n=3), 168 h (n=2). (A-B) Data represent mean \pm SEM. (c) Data represent mean normalized to Control-Ab for the corresponding route of administration. (d) Assay was run in technical quadruplicate (mGIPR-Ab) and triplicate (GIP). cAMP = cyclic AMP; EC_{50} = half-maximal effective concentration; IC_{50} = half-maximal inhibitory concentration; ICV = intracerebroventricular.

A

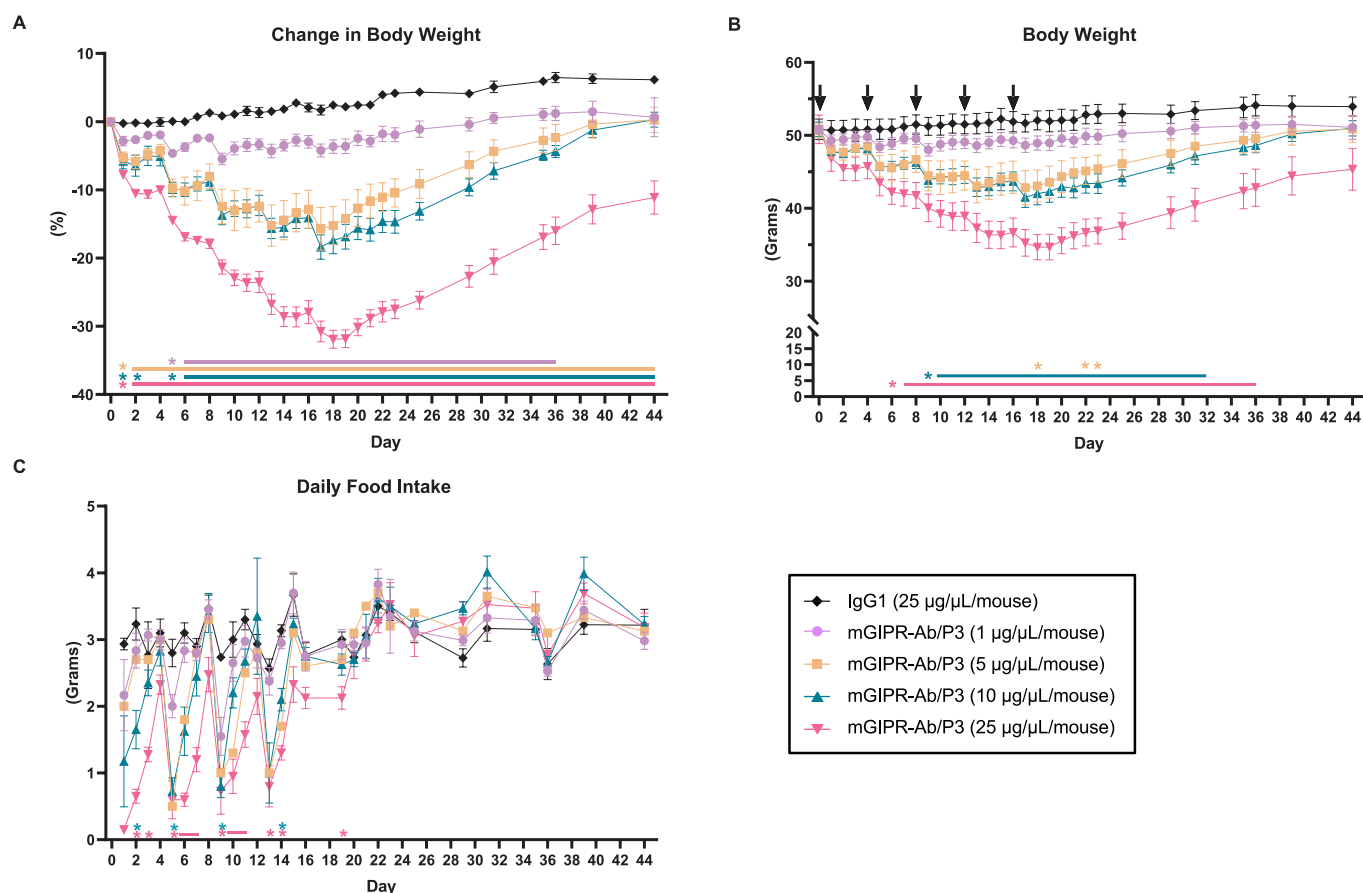
Molecule	Antibody	GIPR IC ₅₀	GLP-1 Analog	GLP-1R EC ₅₀
mGIPR-Ab/P1	Anti-mouse GIPR Ab	1.421e-007	P1 = [Aib ^{8,22} ;Gly ³⁶]GLP-1(7-37)	3.030e-011
mGIPR-Ab/P3 (AMG133 murine surrogate)	Anti-mouse GIPR Ab	1.474e-007	P3 = [Aib ⁸ ;Tyr ¹⁶ ;Glu ²² ;Gly ³⁶]GLP-1(7-37)	2.333e-011



Extended Data Fig. 2 | mGIPR-Ab/P1 and mGIPR-Ab/P3 have similar in vitro potency and comparable effects on cAMP activity. Potency and relative activity of mGIPR-Ab/P1 and mGIPR-Ab/P3 were compared in vitro. **(a)** GIPR IC₅₀ and GLP-1R EC₅₀ are comparable with both molecules, despite different GLP-1 analogs

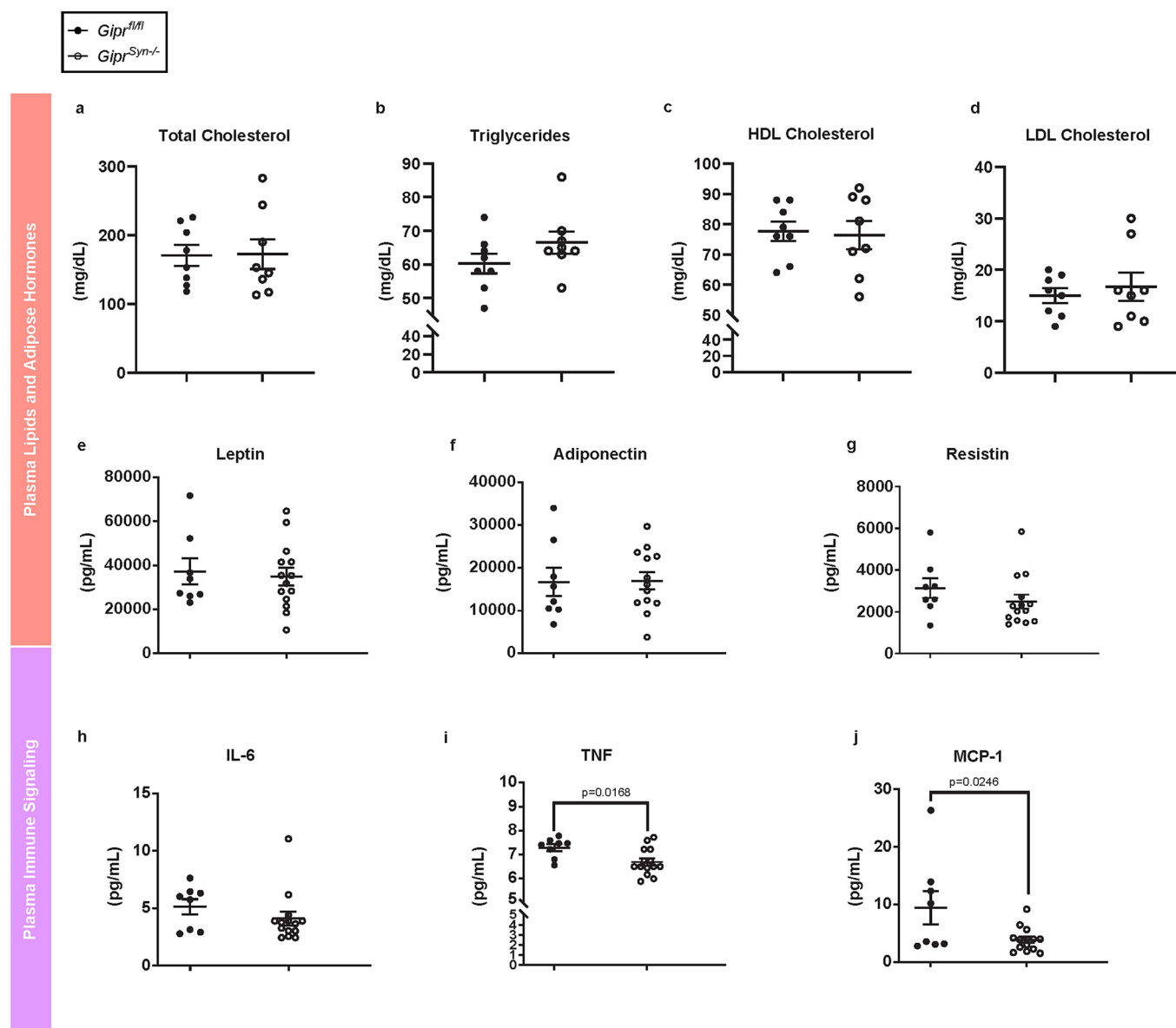


used. **(b)** mGIPR-Ab/P1 and mGIPR-Ab/P3 have identical curves in a GIPR cAMP antagonist assay in 293 T hGIPR-expressing cells, as well as in **(c)** GLP-1R cAMP agonist assay in CHOK1 hGLP-1R-expressing cells. Assay was run in technical duplicates. cAMP = cyclic AMP; CHO = Chinese hamster ovary.



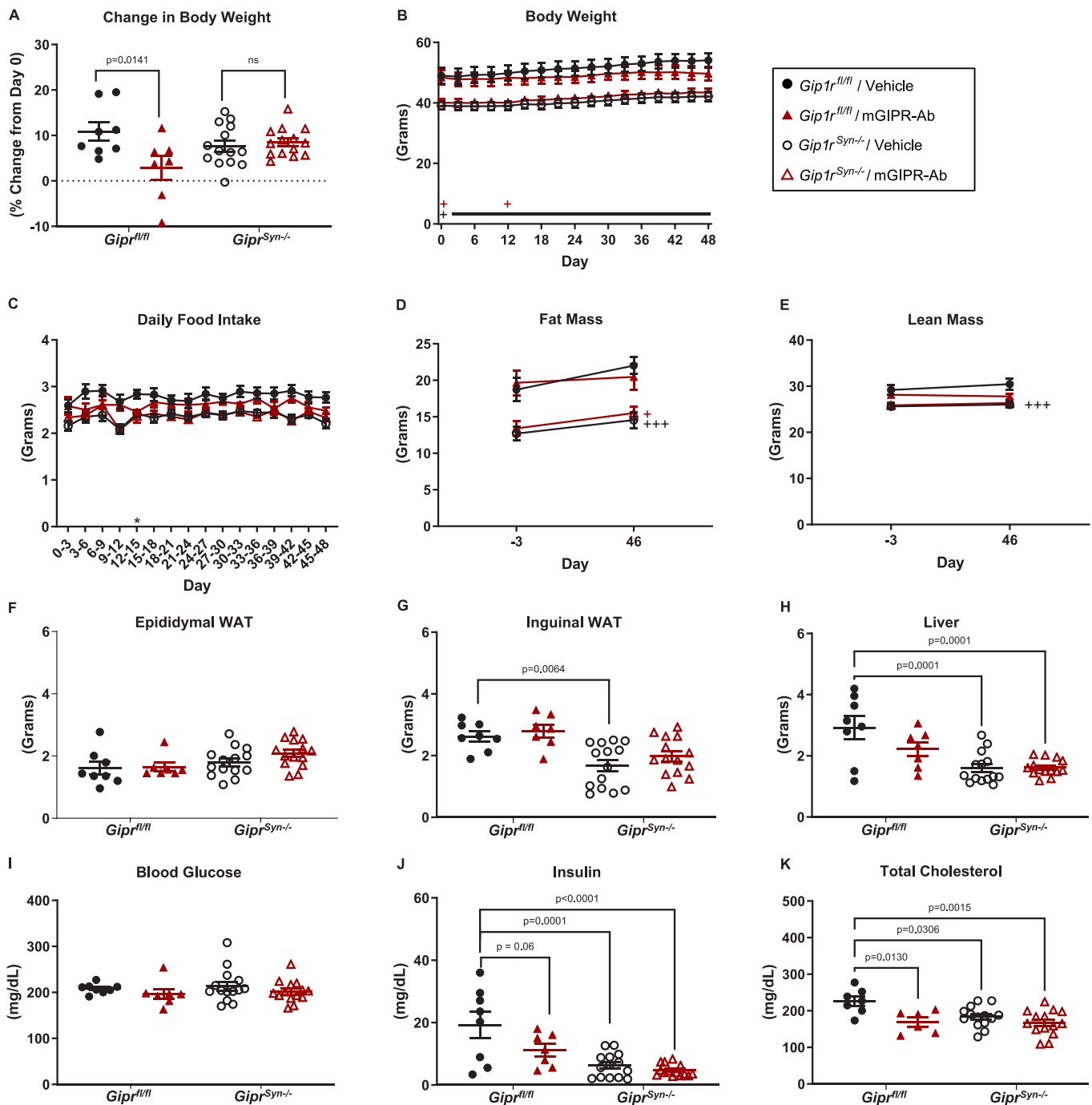
Extended Data Fig. 3 | Central administration of mGIPR-Ab/P3 peptide-antibody conjugate induces sustained weight loss in obese mice. ICV-cannulated DIO mice were randomized into groups to receive 25 µg/µL/mouse IgG1 or 1, 5, 10, or 25 µg/µL/mouse mGIPR-Ab/P3. Mice were dosed ICV every 4 days for 5 treatments. (a) Percent change in body weight from day 0, (b) body weight, and (c) food intake was measured up to 44 days. (A-C) 25 µg/µL/mouse

IgG1 (n=5), 1 µg/µL/mouse mGIPR-Ab/P3 (n=6), 5 µg/µL/mouse mGIPR-Ab/P3 (n=6), 10 µg/µL/mouse mGIPR-Ab/P3 (n=6), or 25 µg/µL/mouse mGIPR-Ab/P3 (n=6). (A-B) Two-way ANOVA with Tukey's test for multiple comparisons, (C) mixed-effects analysis with Tukey's test for multiple comparisons, * $p < 0.05$ vs. IgG1 control. Data represent mean \pm SEM. ANOVA = Analysis of Variance; DIO = diet-induced obese; ICV = intracerebroventricular.



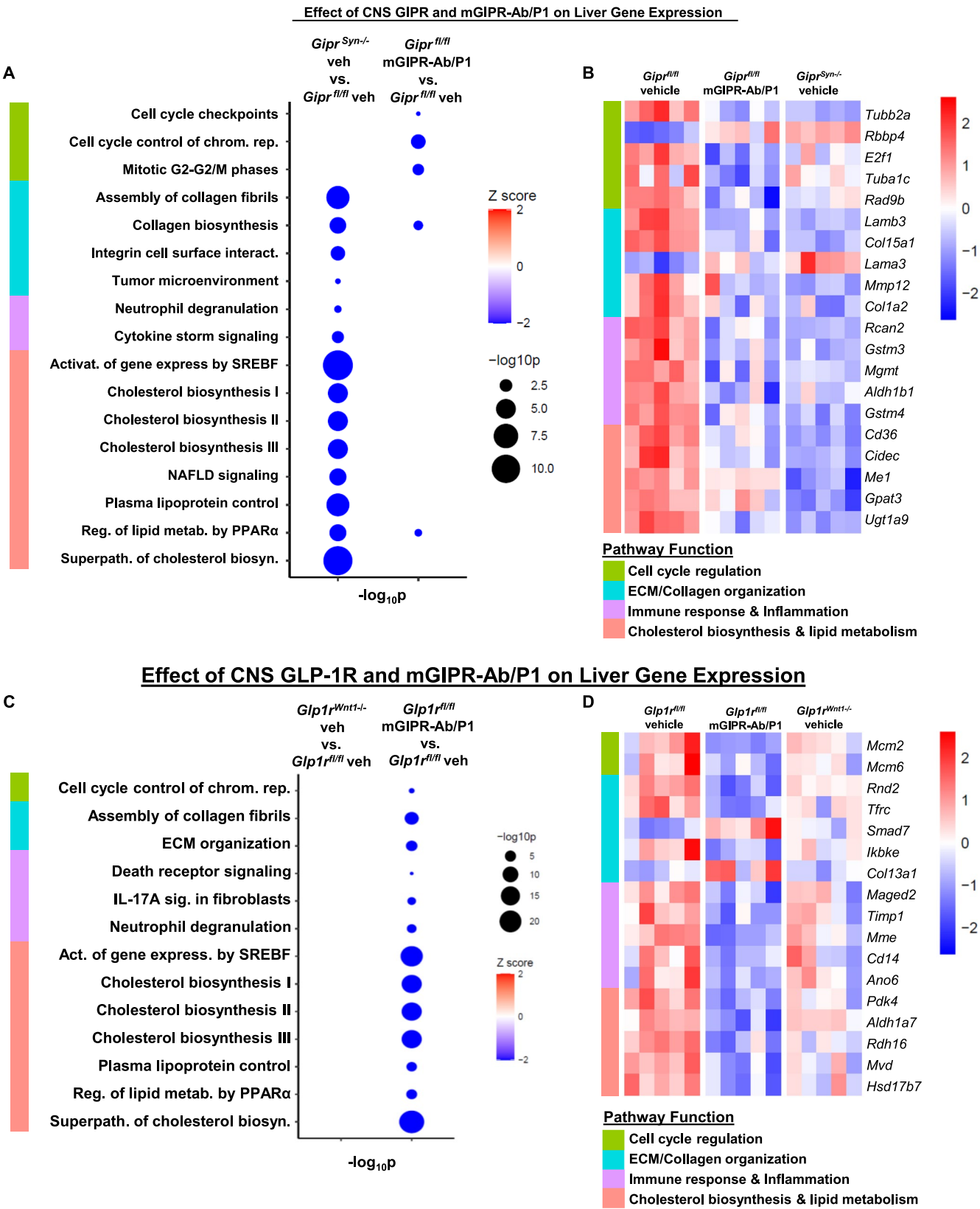
Extended Data Fig. 4 | Characterization of CNS GIPR Knockout mice. Plasma biomarker levels were assessed in two separate cohorts of mice. Plasma (a) total cholesterol, (b) triglycerides, (c) high density lipoprotein (HDL) cholesterol, and (d) low density lipoprotein (LDL) cholesterol were measured in $Gipr^{fl/fl}$ (n=8) and $Gipr^{syn-/-}$ mice (n=8). In a separate cohort (given sample constraints),

plasma levels of (e) leptin, (f) adiponectin, (g) resistin, (h) Interleukin-6 (IL-6), (i) tumor necrosis factor alpha (TNF), and (j) monocyte chemoattractant protein-1 (MCP-1) were measured in $Gipr^{fl/fl}$ (n=8) and $Gipr^{syn-/-}$ (n=14) mice. (A-J) Two-tailed unpaired t test. * $p < 0.05$, ** $p < 0.01$, *** $p < 0.001$, **** $p < 0.0001$ vs. $Gipr^{fl/fl}$ control.



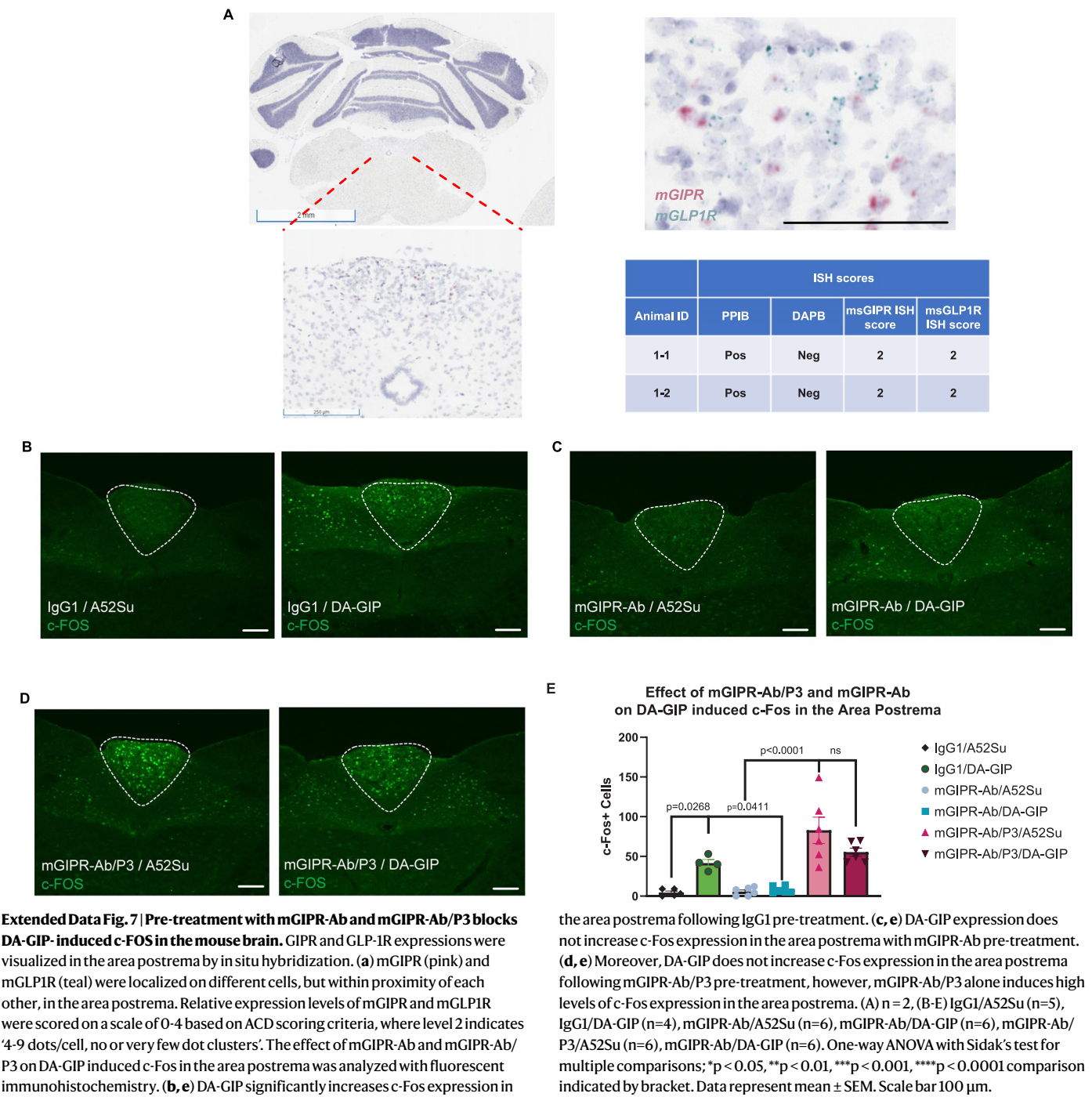
Extended Data Fig. 5 | GIPR CNS KO mice are resistant to mGIPR antibody treatment. Male *Gipr*^{fl/fl} and *Gipr*^{Syn-/-} littermates were fed HFD for 13 weeks and then treated with vehicle (2 mL/kg) or mGIPR-Ab (25 mg/kg) every 6 days for 48 days. (a) Day 48 % change in body weight, (b) body weight over time, and (c) average daily food intake measured every 3 days. Body composition measured by MRI (d) fat mass and (e) lean mass on days -3 and 46. Day 48 necropsy tissue weights (f) epididymal WAT, (g) inguinal WAT, and (h) liver. Day 48 4-hour fasted (i) blood glucose, (j) plasma insulin, and (k) plasma total cholesterol.

(A–K) *Gipr*^{fl/fl} / Vehicle (n=8), *Gipr*^{fl/fl} / mGIPR-Ab (n=7), *Gipr*^{Syn-/-} / Vehicle (n=14), *Gipr*^{Syn-/-} / mGIPR-Ab (n=14). (A, D–K) One-way ANOVA with Tukey's test for multiple comparisons, (B–C) Two-way repeated measures ANOVA or mixed-effects analysis with Tukey's test for multiple comparisons. *p < 0.05, **p < 0.01, ***p < 0.001, ****p < 0.0001 vs. vehicle within genotype or comparison indicated by bracket; + (black) vs. *Gipr*^{fl/fl} within vehicle; + (red) vs. *Gipr*^{fl/fl} within mGIPR-Ab treatment. Data represent mean ± SEM.



Extended Data Fig. 6 | mGIPR-Ab/P1 treatment and CNS GIPR KO result in gene expression profile changes in liver. Transcriptomic analysis was conducted on liver tissues from *Gipr^{fl/fl}*, *Gipr^{Syn-/-}*, *Glp1r^{fl/fl}* and *Glp1r^{Wnt1-/-}* mice treated with either vehicle or mGIPR-Ab/P1. Samples were analyzed for differential gene expression (DEG) using DESeq2 and Ingenuity Pathway Analysis was used to identify most significantly affected pathways. Bubble plot representing pathways enriched for DEGs in (a) *Gipr^{Syn-/-}* vehicle-treated and *Gipr^{fl/fl}* mGIPR-Ab/P1-treated mice, and (c) *Glp1r^{Wnt1-/-}* vehicle-treated and *Glp1r^{fl/fl}* mGIPR-Ab/P1-treated mice.

Size of bubble represent p-value and color shade of bubble represent z-score/enrichment score for each pathway. Heat map for top 5 genes per enriched pathway in (b) *Gipr^{Syn-/-}* vehicle-treated and *Gipr^{fl/fl}* mGIPR-Ab/P1-treated mice, and (d) *Glp1r^{Wnt1-/-}* vehicle-treated and *Glp1r^{fl/fl}* mGIPR-Ab/P1-treated mice. Top 5 genes were selected based off biological relevance and statistical significance. (A,C) Right-tailed Fisher's Exact Test. n=5/group. Chrom = chromosomal, activat. = activation, metab. = metabolism, superpath. = superpathway, biosyn. = biosynthesis.



Reporting Summary

Nature Portfolio wishes to improve the reproducibility of the work that we publish. This form provides structure for consistency and transparency in reporting. For further information on Nature Portfolio policies, see our [Editorial Policies](#) and the [Editorial Policy Checklist](#).

Statistics

For all statistical analyses, confirm that the following items are present in the figure legend, table legend, main text, or Methods section.

n/a Confirmed

- ☐ ☒ The exact sample size (n) for each experimental group/condition, given as a discrete number and unit of measurement
- ☐ ☒ A statement on whether measurements were taken from distinct samples or whether the same sample was measured repeatedly
- ☐ ☒ The statistical test(s) used AND whether they are one- or two-sided
Only common tests should be described solely by name; describe more complex techniques in the Methods section.
- ☒ ☐ A description of all covariates tested
- ☒ ☐ A description of any assumptions or corrections, such as tests of normality and adjustment for multiple comparisons
- ☐ ☒ A full description of the statistical parameters including central tendency (e.g. means) or other basic estimates (e.g. regression coefficient) AND variation (e.g. standard deviation) or associated estimates of uncertainty (e.g. confidence intervals)
- ☐ ☒ For null hypothesis testing, the test statistic (e.g. F , t , r) with confidence intervals, effect sizes, degrees of freedom and P value noted
Give P values as exact values whenever suitable.
- ☒ ☐ For Bayesian analysis, information on the choice of priors and Markov chain Monte Carlo settings
- ☒ ☐ For hierarchical and complex designs, identification of the appropriate level for tests and full reporting of outcomes
- ☒ ☐ Estimates of effect sizes (e.g. Cohen's d , Pearson's r), indicating how they were calculated

Our web collection on [statistics for biologists](#) contains articles on many of the points above.

Software and code

Policy information about [availability of computer code](#)

Data collection No code was used.

Data analysis Preclinical data were analyzed using GraphPad Prism 8.4.3. PK measurements generated using Watson LIMS software (ThermoFisher, v.7.4). RNA-sequencing libraries were generated using Omicsoft OSA alignment software (Qiagen) and GenCode (v28) gene models. Transcriptomic analysis was conducted using DESeq2 and Ingenuity Pathway Analysis (Qiagen, v. 111725566), and bubble plots and heatmaps are generated by R packages ggplot2 (3.4.3) and pheatmap (1.0.12). c-Fos image processing was performed with Python and Elastix software, and graphs were generated with Imaris version 2 (Oxford instruments). Area postrema c-Fos IHC imaged using Leica LAS X software.

For manuscripts utilizing custom algorithms or software that are central to the research but not yet described in published literature, software must be made available to editors and reviewers. We strongly encourage code deposition in a community repository (e.g. GitHub). See the Nature Portfolio [guidelines for submitting code & software](#) for further information.

Data

Policy information about [availability of data](#)

All manuscripts must include a [data availability statement](#). This statement should provide the following information, where applicable:

- Accession codes, unique identifiers, or web links for publicly available datasets
- A description of any restrictions on data availability
- For clinical datasets or third party data, please ensure that the statement adheres to our [policy](#)

All source data has been provided.

Research involving human participants, their data, or biological material

Policy information about studies with [human participants or human data](#). See also policy information about [sex, gender \(identity/presentation\), and sexual orientation](#) and [race, ethnicity and racism](#).

Reporting on sex and gender N/A

Reporting on race, ethnicity, or other socially relevant groupings N/A

Population characteristics N/A

Recruitment N/A

Ethics oversight N/A

Note that full information on the approval of the study protocol must also be provided in the manuscript.

Field-specific reporting

Please select the one below that is the best fit for your research. If you are not sure, read the appropriate sections before making your selection.

☒ Life sciences ☐ Behavioural & social sciences ☐ Ecological, evolutionary & environmental sciences

For a reference copy of the document with all sections, see [nature.com/documents/nr-reporting-summary-flat.pdf](https://www.nature.com/documents/nr-reporting-summary-flat.pdf)

Life sciences study design

All studies must disclose on these points even when the disclosure is negative.

Sample size	No statistical methods were used to pre-determine sample sizes for preclinical experiments, but our sample sizes are similar to those reported in previous publications (PMID: 34095876) and based on historical studies/data. We have clearly stated this in the methods section.
Data exclusions	Select food intake data points were excluded from analysis due to food shredding behavior (noted at the time of measurement), so we were unable to obtain accurate measurements for food intake. We have clearly stated this in the methods section.
Replication	Data from Figs. 1-2 were replicated 3x with same results each time. Data from figs. 3-7 each single independent studies, but results were reproducible with similar study designs and test articles.
Randomization	Mice were randomized prior to the start of each study based off of body weight. There were no statistical differences in sorting parameters between groups at the start of each study.
Blinding	In vivo studies were not blinded due to practical and resource constraints. Ex vivo studies were blinded. We have clearly stated this in the methods section.

Reporting for specific materials, systems and methods

We require information from authors about some types of materials, experimental systems and methods used in many studies. Here, indicate whether each material, system or method listed is relevant to your study. If you are not sure if a list item applies to your research, read the appropriate section before selecting a response.

Materials & experimental systems

n/a	Involved in the study
<input type="checkbox"/>	<input checked="" type="checkbox"/> Antibodies
<input type="checkbox"/>	<input checked="" type="checkbox"/> Eukaryotic cell lines
<input checked="" type="checkbox"/>	<input type="checkbox"/> Palaeontology and archaeology
<input type="checkbox"/>	<input checked="" type="checkbox"/> Animals and other organisms
<input checked="" type="checkbox"/>	<input type="checkbox"/> Clinical data
<input checked="" type="checkbox"/>	<input type="checkbox"/> Dual use research of concern
<input checked="" type="checkbox"/>	<input type="checkbox"/> Plants

Methods

n/a	Involved in the study
<input checked="" type="checkbox"/>	<input type="checkbox"/> ChIP-seq
<input checked="" type="checkbox"/>	<input type="checkbox"/> Flow cytometry
<input checked="" type="checkbox"/>	<input type="checkbox"/> MRI-based neuroimaging

Antibodies

Antibodies used	PK assays utilized the following monoclonal antibodies: biotinylated human GIPR (Amgen Inc; Lot # 19457-1), ruthenylated mouse anti-human Fc (Amgen Inc.; Lot # 43509-4). PK was analyzed with ECL-based immunoassay. Whole brain IgG biodistribution and cFos staining utilized the following antibodies: rabbit anti-cFos, Cell Signaling, ab2250S; donkey anti-rabbit Cy5, Jackson ImmunoResearch; donkey anti-human AF790, Jackson ImmunoResearch. AP c-Fos immunohistochemistry utilized the following antibodies: rabbit anti-c-Fos (Synaptic Systems, Cat 226 008), Goat anti-rabbit AF Plus 488 (Invitrogen, Cat A32731).
Validation	Antibodies were validated and dilutions optimized internally with both positive and negative controls in separate studies. Antibodies were validated in mouse tissues with known expression of mRNA/protein.

Eukaryotic cell lines

Policy information about [cell lines and Sex and Gender in Research](#)

Cell line source(s)	CHO cells stably expressing human GLP-1R and HEK293T cells stably expressing human GIPR were generated at Amgen Inc. Neuro2a mouse cell line from ATCC.
Authentication	Cell lines were not independently authenticated.
Mycoplasma contamination	All cell lines tested negative for mycoplasma contamination.
Commonly misidentified lines (See ICLAC register)	None.

Animals and other research organisms

Policy information about [studies involving animals; ARRIVE guidelines](#) recommended for reporting animal research, and [Sex and Gender in Research](#)

Laboratory animals	All research protocols were reviewed and approved by the Amgen Institutional Animal Care and Use Committee (Thousand Oaks, CA), Toronto Centre for Phenogenomics at Mount Sinai Hospital (Toronto, Canada), as well as the Danish Animal Experimentation Council. Lighting in animal holding rooms was maintained on 12:12 hr light:dark cycle, and the ambient temperature and humidity range was at 68-79 °F and 30-70%, respectively. Animals had ad libitum access to irradiated pelleted feed and reverse-osmosis chlorinated (0.3 to 0.5 ppm) water via an automatic watering system. Male diet induced obese (DIO) C57Bl/6 mice (Envigo or Jackson); male Gipr fl/fl and Gipr syn ^{-/-} (Charles River Laboratories); male Glp1r fl/fl and Glp1r wnt1 ^{-/-} (Mount Sinai Hospital). All mice were ~24 weeks old at start of study.
Wild animals	No wild animals were used in this study.
Reporting on sex	Most studies were conducted in male mice, which is specified in the results, methods, and figure legends. One study (figure 5) was conducted using male and female mice.
Field-collected samples	No field-collected samples were used in this study.
Ethics oversight	All mice were housed at an AAALAC, International accredited facility. Animals were cared for in accordance with the Guide for the Care and Use of Laboratory Animals, 8th Edition. All research protocols were reviewed and approved by the Amgen Institutional Animal Care and Use Committee and Amgen External Study Ethical Review Committee (ESERC) (Thousand Oaks, CA), Toronto Centre for Phenogenomics at Mount Sinai Hospital (Toronto, Canada), and Danish Animal Experimentation Council (Hørsholm, Denmark). Lighting in animal holding rooms was maintained on 12:12 hr light:dark cycle, and the ambient temperature and humidity range was at 68-79 °F and 30-70%, respectively. Animals had ad libitum access to irradiated pelleted feed and reverse-osmosis chlorinated (0.3 to 0.5 ppm) water via an automatic watering system.

Note that full information on the approval of the study protocol must also be provided in the manuscript.

Plants

Seed stocks	N/A
Novel plant genotypes	N/A
Authentication	N/A